



UNIVERSITÀ
DEGLI STUDI
DI PADOVA

Università degli Studi di Padova

Dipartimento dei Beni Culturali: Archeologia,
Storia dell'Arte, del Cinema e della Musica

Master's degree in
ARCHAEOLOGICAL SCIENCES

Curriculum in
APPLIED SCIENCES TO CULTURAL HERITAGE MATERIALS
AND SITES

Constructing Patavium:

Exploitation of Local Resources in the Ancient Mortars of Montegrotto Terme, Italy

Supervisor:

Dr. Michele Secco

Co-supervisor:

Dr. Simone Dilaria

Co-supervisor:

Dr. Caterina Previato

Master Candidate

Emma Katelyn “Milo” Pilgrim

2070768

ACADEMIC YEAR 2023/2024

Table of Contents

Table of Contents	2
Acknowledgments	4
Abstract Sommario	5
1. Introduction	7
1.1 Patavium & Aquae Patavinae (Montegrotto Terme)	8
1.2 Geological Resources of the Euganean Hills	11
1.3 Mortars in Antiquity: <i>Opus Caementicium</i>	11
1.4 Identifying Sites of Ancient Pozzolan Extraction	13
2. Sites and Samples	16
2.1 Montegrotto Terme: Via degli Scavi	16
2.2 The Villa Draghi Quarry Site	23
3. Scientific Methods	25
3.1 Petrographic Analysis	25
3.2 XRPD:	25
3.3 Wet Gravimetric Separation of the Binder Fraction	27
3.4 SEM-EDS	27
3.5 XRF	28
4. Results	31
4.1 Petrographic Analysis of Selected Montegrotto Samples	31
4.2 XRPD:	39
4.2.1 Bulk Mortars	39
4.2.2 Volcanic Aggregates & Geological Samples	41
4.3 SEM-EDS	42
MG02	43
MG11	45

MG10	48
MG12	50
4.4 Results of Binder Fractions	52
4.4.1 XRPD	52
4.4.2 SEM-EDS	52
MG01 Binder	54
MG05 Binder	55
MG10 Binder	56
4.5 XRF	57
5. Discussion	61
6. Conclusion	63
7. References	64
8. List of Figures	69
9. List of Tables	72

Acknowledgments

I would like to express my deepest gratitude to my supervisors: Prof. Michele Secco, Dr. Simone Dilaria, and Prof. Caterina Previato. Their passion for archaeology and the applications of modern scientific analysis have shaped my career and allowed me to explore the ancient Mediterranean world in new ways.

I thank the faculty of the Department of Geosciences and the Department of Cultural Heritage for their mentorship in this experimental graduate program. Their generosity of resources allowed me to apply analytical techniques first-hand.

To Alice, Ephrata, Madeline, Marta, and Nicole: thank you all for your support and encouragement.

To my family who supported my studies from afar.

Abstract | Sommario

The Via degli Scavi archeological site in Montegrotto Terme, in the province of Padova, provides a unique opportunity to interpret a facet of the Roman construction industry due to its proximity to the geological extraction points of its building materials. The surviving structures boast thick foundations of *opus caementicium*, a hydraulic lime mortar mixed with fine and coarse aggregate that hardens with monolithic properties. Combined with a series of field surveys, newly discovered quarry sites may provide insight to the evolution of building material in ancient northern Italy.

Using Montegrotto Terme's Via degli Scavi archeological site as a case study of Roman pozzolanic construction, the mineralogy and chemistry of reactive aggregates are compared to raw pyroclastic material sampled from identified zones of ancient quarrying in the Euganean Hills. The qualities of *opus caementicium* samples from various structures within the thermal context reveal the diverse technologies exploited in antiquity.

Through a series of archeometric analyses, it is determined that both ceramic-based and volcanic breccia-based aggregates were used to create the mortars at the site. Thin sections studied under optical microscope provide generalized understanding of the physical makeup of the mortars. Bulk analysis of mortar through X-Ray Powder Diffraction (XRPD) and X-ray fluorescence (XRF) characterized the mineralogy and geochemistry of the samples. Binder fraction was studied independently using wet gravimetric separation techniques. Study by scanning electron microscopy-energy dispersive spectroscopy SEM-EDS highlighted the mineralogical results of intentional reactive aggregate selection and the reactivity of the calcic binder.

Provenance of volcanic aggregate was determined from XRF results using multivariate statistical processing and linear discriminant analysis (LDA).

This work is part of a larger project to understand the use of the Euganean Hills in antiquity and to discover the industrial pathways that link the modern city of Padova's Roman architecture to its raw materials.

Il sito archeologico di Via degli Scavi a Montegrotto Terme, in provincia di Padova, offre un'opportunità unica per interpretare l'articolazione dell'industria edile romana grazie alla sua vicinanza ai punti di estrazione geologica dei suoi materiali da costruzione. Le strutture sopravvissute vantano spesse fondamenta di *opus caementicium*, una malta di calce idraulica mescolata con aggregati fini e grossolani che indurisce con proprietà monolitiche. In combinazione con una serie di indagini sul campo, siti di recente scoperta identificabili come cave antiche possono fornire informazioni sull'evoluzione dei materiali da costruzione nell'antica Italia settentrionale.

Utilizzando il sito archeologico di Via degli Scavi di Montegrotto Terme come caso di studio di costruzione pozzolanica romana, la mineralogia e la chimica degli aggregati reattivi sono state confrontate con il materiale vulcanico campionato da zone identificate come cave antiche nei Colli Euganei. Le qualità dei campioni di *opus caementicium* provenienti da varie strutture nel contesto termale rivelano le diverse tecnologie sfruttate nell'antichità.

Attraverso una serie di analisi archeometriche, si è stabilito che per creare le malte nel sito sono stati utilizzati sia aggregati ceramici che vulcanici a base di breccia. Le sezioni sottili studiate al microscopio ottico hanno fornito una comprensione generalizzata della composizione fisica delle malte. L'analisi in massa della malta tramite diffrazione ai raggi X delle polveri (XRPD) e fluorescenza a raggi X (XRF) hanno permesso di caratterizzare la mineralogia e la geochimica dei campioni. La frazione legante è stata studiata in modo indipendente utilizzando tecniche di separazione gravimetrica a umido. Lo studio mediante microscopia elettronica a scansione-spettrocopia a dispersione di energia SEM-EDS ha evidenziato una selezione intenzionale di aggregati reattivi e la reattività del legante calcico stesso.

La provenienza degli aggregati vulcanici è stata dedotta dai risultati XRF utilizzando l'elaborazione statistica multivariata e l'analisi discriminante lineare (LDA).

Questo lavoro fa parte di un progetto più ampio per comprendere lo sfruttamento delle georisorse dei Colli Euganei nell'antichità e per scoprire i percorsi industriali che collegano l'architettura romana della moderna città di Padova alle sue materie prime.

1. Introduction

In the shadow of the Alps, the Euganean Hills are a sudden outburst of volcanic rock in the otherwise flat Po Plain of northern Italy. While the exploitation of the Euganean Hills' geological resources dates well into prehistory, its intensive use began with the Roman conquest of the territory. To understand the technical applications of these geological materials in antiquity, particularly the use of Euganean pozzolanic materials in Roman concrete mixtures, this project merges history and material science to characterize ancient mortars from the Via degli Scavi archeological site in Montegrotto Terme (the ancient Aquae Patavinae) and pinpoint the precise geological origin of their reactive aggregates by comparison to geological resources from the Euganean Hills.



Figure 1: Topographic map of Italy with the Veneto shaded in pink and the Euganean Hills marked in white.

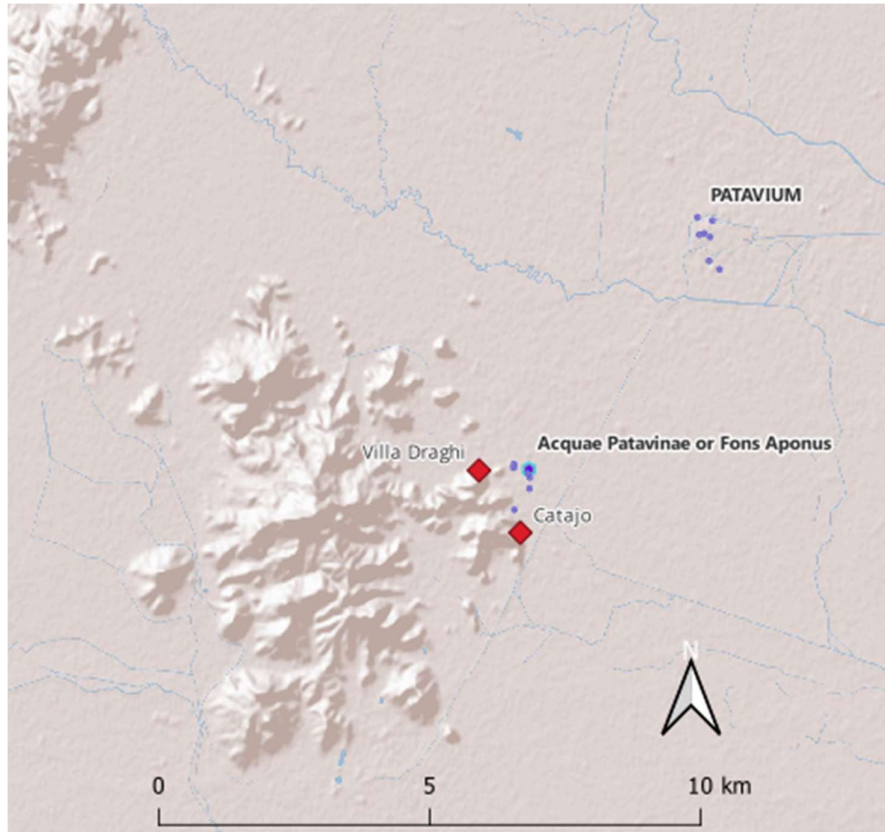


Figure 2: Morphological map of the Euganean Hills with the known Roman archeological sites of Patavium and Aquae Patavinae marked in blue. Two potential ancient quarry sites, Villa Draghi and Catajo, are marked by red diamonds. The Euganean hills are to the southwest of modern Padova and west of the Venetian Lagoon.

1.1 Patavium (Padova) & Aquae Patavinae (Montegrotto Terme)

The archaeological site of Aquae Patavinae (the modern town of Montegrotto Terme) lies outside the ancient city known by the Romans as Patavium (the modern city of Padova). The initial settlement of the region predates the romanization of northern Italy and boasts a foundational myth mirroring that of Rome. The Euganean tribes for which the nearby hills were named settled before the Gaul invasions of the 5th Century BCE. They were eventually outmaneuvered by the Veneti, a group mythologically founded by Trojan refugees under the leadership of Antenor, who fled to Italy on an alternate path from Aeneas (Vergil Aeneid, 1.242). Patavium grew on the banks of the river Medoacus (Gasparotto 1928) whose navigable waters allowed a rich network of trade within the Adriatic.

Livy describes the Venetian lagoon and the ancient Patavians as a formidable power in the northern Adriatic by 302 BCE. Livy, as a native Patavian, may have accessed historical records unknown to contemporary scholars in Rome. Alternatively,

Livy may have preserved local legends that had not widely spread into the myths of the empire.

Strabo writes that the area of Patavium was a large settlement in a marshy environment (Str. 5.1.7). Estimates of population in the early imperial period place it as the largest city in the region. The Via Annia connected Patavium to Altinum and Atria, and an unnamed route connected Patavium to Vicetia. Traces of the ancient agricultural industry remain most prominently in the countryside surrounding modern Padova: the persistence of geometric plots in the dimensions of Roman centuriation are visible today on the ground and by satellite imagery (Turchetto 2023).

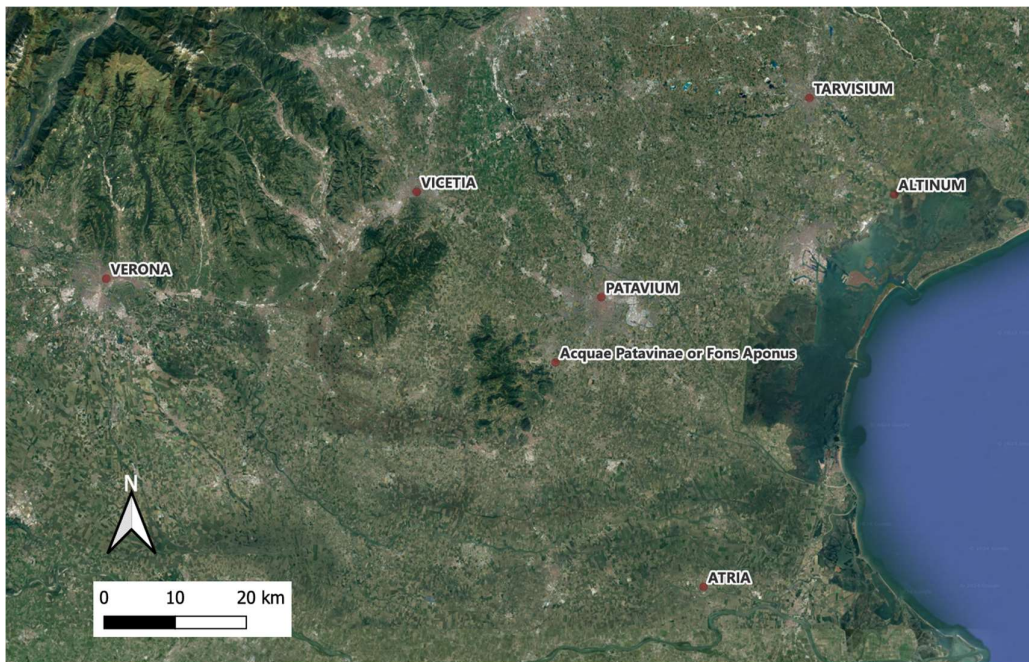


Figure 3: Satellite imagery of northern Italy with Roman city names highlighted.

Gallieno writes that in 260 CE the area was invaded, and shortly after the Goths and Vandals sacked the entire Veneto region. It is said that when Attila the Hun invaded circa 450 CE, the residents of Patavium and nearby cities fled to the small islands in the marshy lagoon that would become the city of Venice (Gasparotto 1928). However, Patavium and many of its neighbors recovered and reestablished themselves under the rule of the Ostrogoth King Theodric the Great by 493. The modern city of Padova and its surrounding towns are dominated by medieval and early modern structures that rest atop archeological deposits from antiquity.

The site of Aquae Patavinae to the west of Patavium boasts an expansive system of thermal waters used for cultural and medicinal purposes since prehistory. Averaging

approximately 80 degrees Celsius, the consistent waters encouraged industries of luxury and leisure. The town rests on the fluvial plain of the Brenta River whose depositional actions brought nutrients and minerals from the Alps. This fertile soil allowed for productive cultivation, as persistence of centuriation attests to the millennia of agricultural practices.

Several ancient sources mention the thermal bath complexes near Patavium: Pliny the Elder referred to the site as *Patavium aquis caldis* (Plin. II 103.227) and *Patavinis fontibus* (Plin. XXXI 6.61). The springs were attributed to the god Aponus by the Veneti tribe, according to Suetonius (Suet. Tib. 14). Suetonius noted that on his way to Illyricum, Tiberius in his obsession with prophecy turned to the oracle of Geryon in the vicinity of Patavium and was recommended to throw gold dice into the fountain of Aponus to see his fortune. His favorable cast told of victory on his march to defeat the Illyrians. Suetonius claimed that one could still witness the miraculous dice at the bottom of the fountain years later: such was the importance of the waters of Aponus, called *Aquae Patavinae* or *Fons Aponi*. The Romans cherished the area of Montegrotto Terme as a thermal retreat and built large structures for health tourism and spiritual associations of the allegedly healing waters. Though the site was hailed as the home of the god Aponus, it is also associated with Apollo as the god of healing. Many surviving *stele* from the region call upon these gods to grant health and prosperity.

In his *Natural History*, Pliny the Elder describes the use of healing mud or salts to deal with excessive fluid in the body. In this, he writes that not all hot springs exhibit medicinal properties; he claims that a test of discoloring bronze or silver does not necessarily disprove the medicinal quality of the springs, as Patavium water is known to not discolor silver (Plin. NH XXXII.6.1). His example of the springs may hint to an early understanding of their minerality. In comparison to the volcanically driven springs in the south of Italy that release odorous hydrogen sulfide, the sodium-chlorinated water and its bromide-iodine minerals appeared miraculous. Unlike their urban counterparts, the many bath complexes in the Euganean Hills maintain a sense of connectivity with the wild divinities that bring their pseudo-medicinal properties, a commercial enterprise that continues to this day.

1.2 Geological Resources of the Euganean Hills

The site of *Aquae Patavinae* lies just beside the Euganean Hills, whose rich natural resources go beyond its hydrothermal basin. The hills are of volcanic origin with two major eruption phases approximately 40 and 33 million years before present. The volcanic activity occurred when the region was submerged under seawater, giving the stratigraphy an interesting lamination of both volcanic and carbonate sedimentary material. These eruptive phases produced rhyolite, trachyte, latite, basalt and their equivalent breccias, whose varied geochemical properties are suitable for a range of construction needs. This geological material has been exploited since antiquity for construction and infrastructural purposes along the Adriatic coast.

Trachyte is an extrusive volcanic rock containing alkali feldspar phenocrysts. An extensive network of quarries, roadways, and canals allowed the movement of extracted trachyte throughout the Po Plain in antiquity (Zara 2018). The Romans exploited Euganean resources in immense quantities, with documented use as far as Fano to the south, Milan to the East, and Aquileia to the north (Zampieri 1994; Zara 2018). Today, trachyte lines the roads of historic towns in the Po River Valley, surviving centuries of wear and waterlogging. It is the most abundant product quarried from the Euganean hills, but other local geological features are proved valuable for construction practices.

Breccia refers to any rock containing crystalline fragments in a finer matrix. The Euganean trachytic breccias, though chemically similar to trachyte, are mineralogically diverse. These volcanic breccias contain large alkaline mineral clasts suspended in an amorphous (glassy) silicate matrix. Due to rapid cooling, the matrix cannot fully develop a crystalline state during its transition from liquid to solid, thus leaving it in an activated state that is susceptible to chemical reaction. This amorphous-rich deposit is an ideal pozzolanic reactive agent required for Roman *opus caementicium*, a hydraulic lime mortar that functions well in inundated environments.

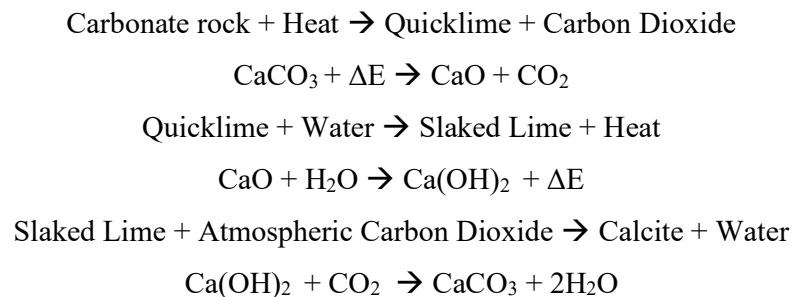
1.3 Mortars in Antiquity: *Opus Caementicium*

Opus caementicium, also known colloquially as Roman concrete, derives its strength from the pozzolanic chemical reaction. Pozzolan now refers widely to any amorphous silicate compound that is used in cement production, but the name derives from the Roman city of *Puteoli* in the Bay of Naples, where volcanic ash was

extensively exploited as *pulvis puteolanus* (Leone et al. 2019). Romans were not the inventors of hydraulic lime binders, but their innovations and the sheer scale of building projects set them apart from earlier civilizations such as the Phoenicians and Minoans, who mainly used the technology for nonstructural plastering (Chiotis et al. 2001). Pozzolanic mortars differ from aerial-lime binders due to the reaction between calcium from the lime and the pozzolan's amorphous silicate (Secco et al. 2018). Because pozzolanic reactions require water, the mortars can consistently set in humid environments, even when permanently inundated. Pozzolanic materials are not exclusively volcanic in origin; crushed ceramic and organic ash were often utilized as they contain sufficient silicates for the pozzolanic reaction to occur and were an accessible alternative to distant or costly geological materials. This crushed ceramic is called *cocciopesto*, and its versatile reuse is also found in the industries of brickmaking and pottery production (Moropoulou et al. 2005). Romans therefore utilized three pozzolanic materials in different circumstances: geological, ceramic, and organic.

The other major reactive substance in *opus caementicium* is calcium hydroxide, known colloquially as slaked lime. In antiquity, the production of slaked lime was a largescale industry as it was an essential ingredient for both structural mortars and superficial plastering. To produce slaked lime, one must first fire geological calcite in a kiln to a temperature above 700 degrees Celsius, ideally up to 900 degrees. This process transforms calcium carbonate (mainly corresponding to the mineral calcite, CaCO_3) into quicklime (CaO) through the release of carbon dioxide (CO_2). The quicklime is crushed into powder and mixed with water to create slaked lime (Ca(OH)_2) (Dilaria and Secco, 2022).

In a typical aerial lime binder, the slaked lime would be allowed to dry. When water escapes as vapor, the system absorbs ambient carbon dioxide and reforms as calcite:



In the production of pozzolanic mortars, the slaked lime is mixed with pozzolan and water. When saturated in a highly alkaline mixture of slaked lime, pozzolans begin to dissolve and form calcium-silicate-hydrate (C-S-H) around their external perimeter (Barnes and Benson 2002). Eventually buckling under the pressure of osmosis, the outer shell will burst and allow the entire pozzolanic particle to dissolve and react with the calcium hydroxide. C-S-H is a chain silicate with greater compressive strength than the calcite in aerial lime mortars, and it is bolstered by its additional products like calcium aluminate hydrates (C-A-H, sometimes called AFm due to their aluminum and iron content). This pozzolanic reaction will continue until either the water or the reactants are completely consumed.

Slaked Lime + Alumina-Silicate + Water → Calcium Silicate Hydrate + Calcium Aluminate Hydrate

A = Al₂O₃, C= CaO H= H₂O, S = SiO₂

CH + AS + H → C-S-H + C-A-H

Opus caementicium is only one of many construction techniques utilized during the Roman Republic and Empire. The complex mortar was often used as a foundation for monumental construction, and its waterproof quality and plasticity made it an ideal material for constructing thermal complexes. By pouring the mixture of mortar, fine sands, and coarse aggregate, the Romans created artificial monolithic supports. It represents most of the material that survives *in situ* at the Via degli Scavi archaeological site: thick walls, hydraulic foundations, and the mortar between bricks that acted as formworks for the pouring of the *opus caementicium*.

1.4 Identifying Sites of Ancient Pozzolanic Extraction

Frequent study of the region provides a high degree of knowledge of the natural characteristics of the hills, and now several areas of interest lie within the Regional Park of the Euganean Hills. With our understanding of local geology, the survey team focused on deposits of rhyolitic and trachytic breccias, as they contain the highest percentage of amorphous silica and are therefore the most reactive aggregates available in the region for a pozzolanic mortar. With the constraint of pozzolanic reactivity, the team narrowed the survey scope to those outcrops that most exhibit the mineralogical properties required for successful aggregates. Some zones experienced continuous

exploitation as quarry activity continued well into the 20th century. This presents an additional challenge: it is possible that many areas that might have once hosted Roman-era quarries were later destroyed, and so archaeological evidence is absent in the present day.

Through satellite imagery, it became apparent that some anthropic indentations in the hills predated the known industrial sites documented in the 20th Century. The University of Padova collaborated with the archeological company ArcheTipo to perform a high-density LiDAR scan, and the data was elaborated by Josiah Olah (Olah 2024, forthcoming). Using a drone, the team surveyed several different hillsides from February to March of 2023. From his digital elaboration, Olah noted several zones of potential anthropic intervention that remained absent from historical maps of the quarries.



Figure 4: Map of the Villa Draghi quarry (red) in relation to archaeological sites of Montegrotto Terme (blue).

Most notably, the Villa Draghi site revealed a series of incised tunnels with traces of cutting by hand. Sporadic ceramic fragments found at the site, such as a fragment of roof tile resembling typical Roman shapes, are a clear indication of the time of use. Though the quarry is now quite filled with deposits loosely sedimented over the ages, one can glimpse sunlight through a sliver towards the back of the first cave. Tunnels may connect between the many incisions on the hillside but are now buried in the debris to a currently unknown depth. A planned geophysical survey using electrical resistivity tomography should reveal the depth of the infilling. The archaeological team

can then assess the feasibility of initiating excavation. Several geological samples were extracted by M. Secco and S. Dilaria along the interior of the cave and the outer wall near the signs of incision.

The proximity of Villa Draghi to the complex of Via degli Scavi would make it the most efficient source of raw material for construction. The stone at Via Draghi is quite friable and visually distinctive from the darker lavas that surround it. This geological compound may contain very high amounts of amorphous silicates that bolster its reactivity with slaked lime. Its ease of visual recognition and pulverization would make it an ideal resource for Roman construction development.

Other outcroppings at Catajo Hill show similar potential for ancient extraction and minimal use post-antiquity, and at the private property of Monticello Hill the team must seek permission to survey an apparent quarry. Many areas in the Euganean Hills match the geological needs for pozzolanic production and the archeological dimensions of Roman industrial sites; however, for the scope of this thesis, with consciousness of the practicality of material transport in antiquity, the quarry at Villa Draghi was selected for mineralogical and chemical comparative analysis.



Figure 5: Photos of the newly discovered Villa Draghi quarry site by author

2. Sites and Samples

The archeological site of Via degli Scavi in Montegrotto Terme (Aqua Patavinae) was chosen due to its proximity to the Villa Draghi Quarry and for its architectural complexity. The objective of this study is to comprehend the use of geological resources from the Euganean Hills as reactive aggregate in structural mortars from Roman times. Through optical microscopy, X-ray diffraction, X-ray fluorescence, and scanning electron microscopy, the mortars were characterized mineralogically and chemically. Particular attention was paid to the coarse aggregates within some samples that could be analyzed geochemically to find geological provenance. These tests were then compared to similar results from the samples of the Villa Draghi quarry site and statistically analyzed within a framework of Euganean Hill geological samples.

2.1 Montegrotto Terme: Via degli Scavi

The wealth of archeological material attests to the continuous anthropic use of the Euganean Hills and their precious waters. From small votive objects to monumental structures, the archeological remains from the towns beneath the Euganean hills offer a glimpse into a thermal respite to ailing Romans. Foundations of great bath complexes and rich villas offer a glimpse of the ancient tourism industry. While creating a modern hotel, the Via Neroniana site revealed a private villa with a thermal bath. Several smaller villas dot the ancient countryside. Of the many discoveries in Montegrotto Terme, the complex of Via degli Scavi is the most relevant. The Marquises Dondi dell'Orologio originally excavated part of the site in 1780, when it was incidentally discovered during the University of Padova's regional survey of the medicinal properties of the thermal springs. The first excavation revealed the three pools, which suffered heavy looting and were subsequently reburied. For over a century, the site was obscured. The theater complex was discovered after the state of Italy purchased property and continued excavations in the 1960's.

The lack of surviving documentation from the original excavations orphaned hundreds of objects now kept in the Padova Civic Museum and in the Venetian National Museum of Archaeology. Records from the University of Padova note the existence of polychromatic marble decoration that have since been lost to looting. The Odeon survives only in its concrete foundations; remnants show the seating area and stage

supports, but all decorative pieces have been stripped for reuse. In the Veneto region, this reuse could have occurred in antiquity or in early medieval times. Beyond the lavish décor and small objects, archaeologists found some infrastructurally informative remains, such as extensive lead piping and aqueduct keys to control the flow of water (Biblioteca Comunale Montegrotto Terme, 1997).

Like most towns of ancient origin, Roman material remains trapped beneath the medieval and modern layers of Montegrotto Terme. Present-day excavation is rare and almost always dictated by emergency interventions. It is unlikely we can fully extract information about ancient *Fons Aponi* from its source, as the exposed fragments of architecture have suffered severe physical degradation and mechanical removal of material. Roman roads and other infrastructural features now hide beneath more modern layers of settlement, though the functions of the sites remain charmingly aligned. Villas rest beneath modern mansions, and thermal bath complexes were uncovered beneath modern recreational facilities. The beauty of Montegrotto Terme's continuous use as a recreational center is also its pitfall as an archaeological repository.

Undoubtedly the Via degli Scavi site featured richly decorated architecture, but like most Roman cities in the Veneto region, it is difficult to ascertain the true scale of splendor as most valuable materials were recycled in later eras. In a recent study of local postclassical fired vessels, marble fragments with provenance around the Mediterranean were found as a temper in coarse ceramic production (Maritan et al, 2021). These diverse marbles match several typologies known in classical antiquity, such as the quarries of Carrara and Paros. It is likely that marble scavenged from the remains of Roman structures in Montegrotto Terme and Padova was crushed to make this coarse ware; it is probable that by the time of the first excavation, the site of Via degli Scavi had already suffered significant material loss. In the National Archaeological Museum of Venice, a beautiful statue of the god Aponus stands regally displaced from his origin. Despite its scattered archaeological finds, the Euganean Hill area maintained its destination status and continues to base its economy on thermal tourism, advantageously proximate to the larger cities of modern Padova and Vicenza.

Today, the archaeological site is left partially exposed to the elements, visible from the street but rarely accessible to the public. The *odeon*, two larger baths, a smaller circular bath, and the hydraulic channels are uncovered, as well as the slightly

disjointed rectangular building to the south. The three pools connected to a waterwheel (*noria*) (structure H) which pumped water to specific baths through the mortared channels. The small building marked Structure D was likely built in a separate phase. Its function is debated due to the inconsistent archaeological record, but it is attributed as a later addition of a Nymphaeum. The mid-Twentieth century Hotel Montecarlo now lies abandoned and decaying on top of the southernmost part of Pool A. Because of modern development, the archaeological zone has not been expanded, so there may be further structures connected to the complex that remain undiscovered.

The Odeon (structure E) measures about twenty-five meters across, with eleven rows of seating. Architectural similarities between the outer wall of the *odeon* of Via degli Scavi and the Zairo Theater in Padova suggest a similar building methodology (Deiana and Previato 2023). The foundation hints to a small structure at the crown of the theater, but the sparse archaeological records do not hint to a potential temple. The structure is the most intact of the site, though only brick and mortar remains. A temporary metallic scaffolding partially protects the *cavea* from rain percolation. Exposed perimeters are sealed with a top coating of modern Portland cement and stone rubble, leaving a recognizable line between the archaeological material and the modern addition. From a conservation standpoint, these covers provide beneficial barriers from the harsher elements and allow the material to remain visible above the soil without intensive alteration. The Veneto region receives ample rainfall, and due to the hazards of climate change and anthropogenic pollutants it is better to prevent direct contact of potentially acidic rains.

Pools A and B are both approximately 30 meters in length. Pool B is capped with semicircular design, while A is rectangular in shape. Pool C's thick, circular walls may have carried a domed ceiling akin to those discovered in Baia, Naples (Yegül 1996) (Sinopoli and Aita 2022). Compared to the Forum and Stabian baths of Pompeii, it is likely that Pool C was the frigidarium.

The possible Nymphaeum, Structure D, rests to the side of the complex and contains beautifully geometric pattern of rooms and apses with a central pool or fountain. Structure D could alternatively represent a sudarium or laconicum as seen in the baths of Pompeii (Nielsen 1999). With its rotunda interior and apses, it presents a more complex interior than the other structures.

The workroom (structure H) and deep enclosure where a *noria* (waterwheel) pumped water connects with an expansive hydraulic system that remain visible after excavation but would have been hidden below ground level in antiquity.

Twelve mortar samples were taken from the structures of Via degli Scavi by M. Secco and S. Dilaria in 2019. Of them, seven represent the *odeon* complex. MG01, MG02, and MG07 come from the internal mortars of the *cavea*. MG03 through 06 are from the external supporting walls. MG04 may have acted as a foundation for a small votive site above the theater, like the Temple of Venus at the Theater of Pompey in Rome.

MG08 was sampled from the external portion of structure D, while MG09 comes from structure H which contained the *noria*. MG10 and MG12 are within the bath complexes C and A, and MG11 represents an exterior wall of bath structure C.

It is unclear if an *apodyterium* (changing room) was present at this site. Due to the urban surroundings, further excavation is not proposed at this time. In the future, improving the cohesion of the site and exploring its context in antiquity may fill the gaps left by early archeologists and modern industry.

For provenience studies, volcanic clasts were removed from mortar samples to be studied as standalone materials. These samples were chosen after petrographic analysis of thin sections.



Figure 6: hypothetical reconstruction of the Via degli Scavi archeological site

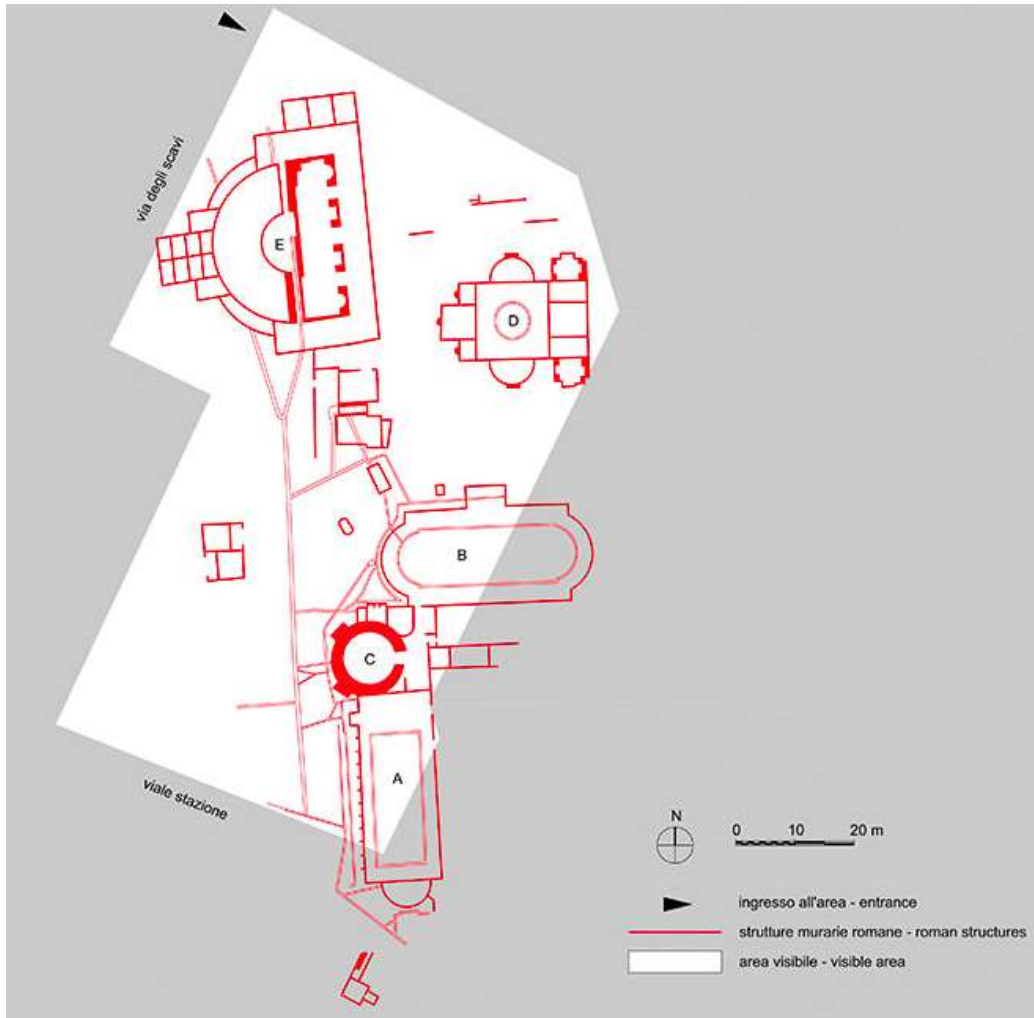


Figure 7: The Site of Via degli Scavi, the ancient Fons Aponi

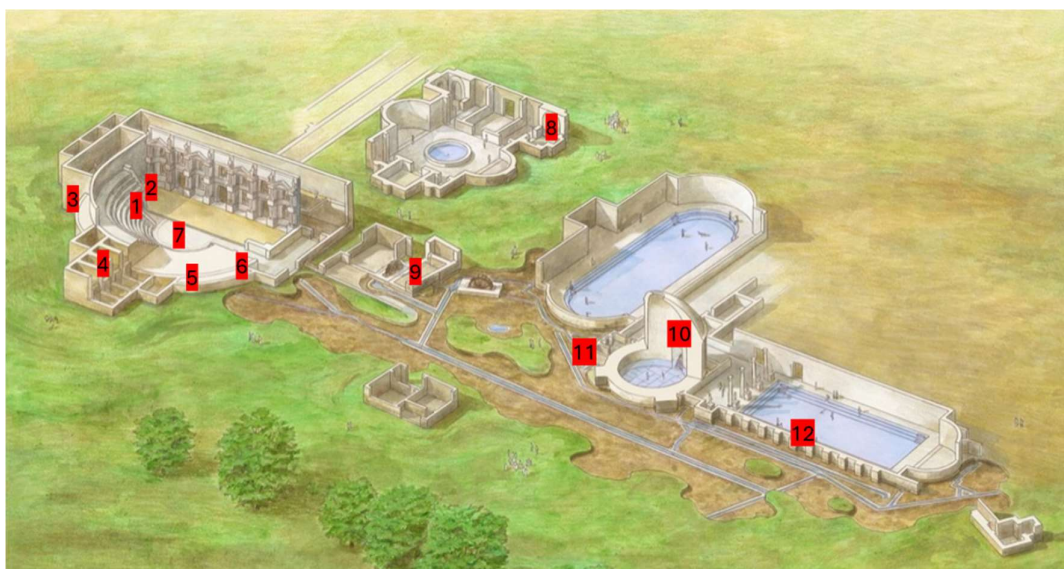


Figure 8: Hypothetical reconstruction of Via degli Scavi site, bottom with sampling points superimposed.

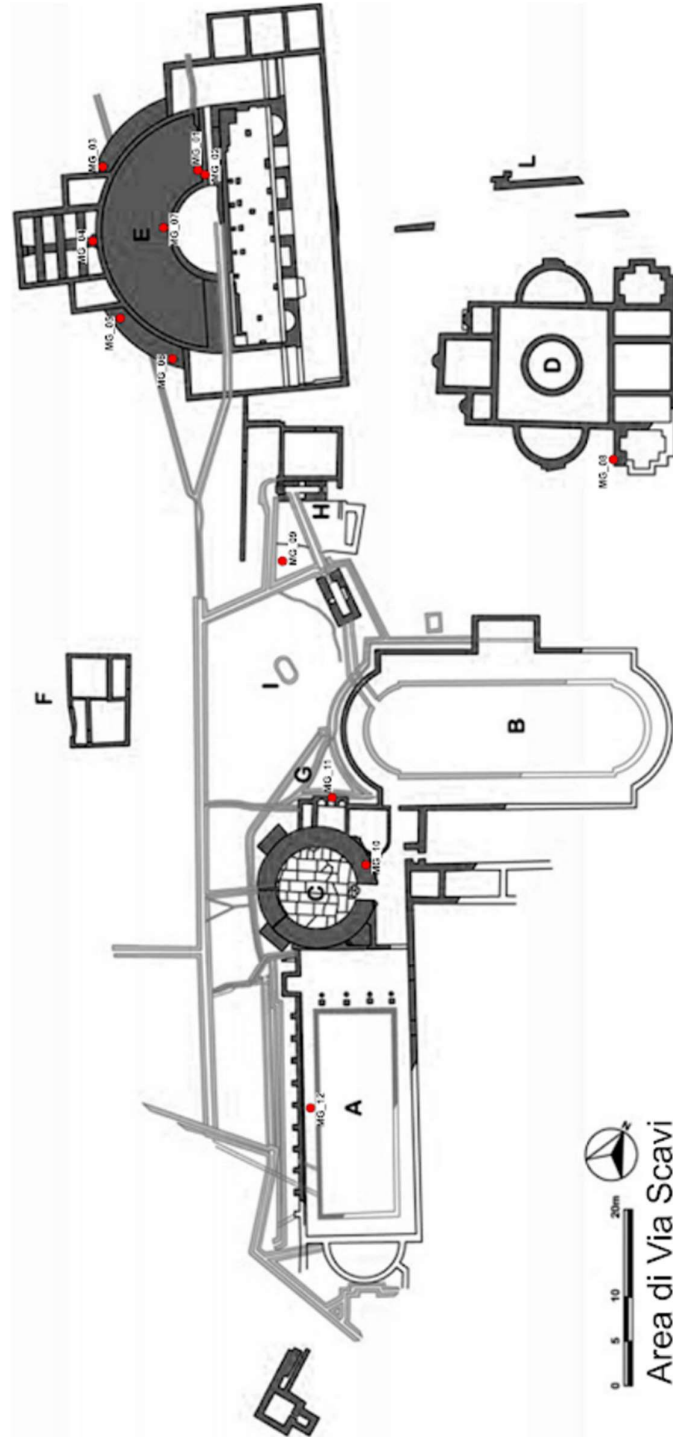
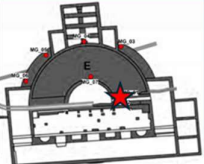

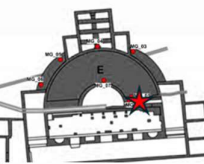

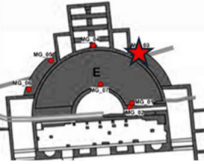

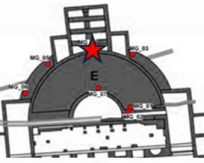

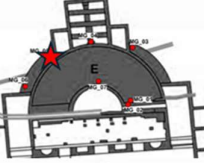

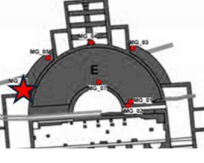

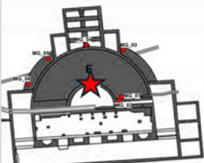

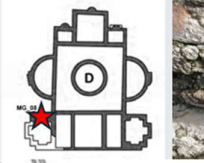





Figure 9: Plan of mortar sampling, by M. Secco and S. Dilaria, University of Padova 2019.

SAMPLE	STRUCTURE	PROPOSED CHRONOLOGY	FUNCTION	SAMPLE LOCATION
MG01	E Theater-temple	1 st Century CE First Phase	STRUCTURAL, cavea of the odeon in opus caementicium	 
MG02	E Theater-temple	2 nd Century CE or later Third Phase	STRUCTURAL, brick partition to reinforce the aditus	 
MG03	E Theater-temple	2 nd Century CE Second Phase	STRUCTURAL, external reinforcement wall of the odeon	 
MG04	E Theater-temple	1 st Century CE First Phase	STRUCTURAL, support walls, potentially for a temple, with brick	 
MG05	E Theater-temple	2 nd Century CE Second Phase	STRUCTURAL, external reinforcement wall of the odeon	 
MG06	E Theater-temple	2 nd Century CE Second Phase	STRUCTURAL, external reinforcement wall of the odeon	 
MG07	E Theater-temple	1 st Century CE First Phase	STRUCTURAL, cavea of the odeon in opus caementicium	 
MG08	D Unknown function	2 nd Century CE Later phase	STRUCTURAL, bedding layer of a perimeter wall	 
MG09	H Noria complex	1 st Century CE First Phase	STRUCTURAL, bedding from a collapsed perimeter wall by the <u>noria</u> structure	 




SAMPLE	STRUCTURE	PROPOSED CHRONOLOGY	FUNCTION	SAMPLE LOCATION
MG10	C Pool basin	1 st Century CE First Phase	STRUCTURAL, cement core of a perimeter wall	
MG11	C Pool structure	1 st Century CE First Phase	STRUCTURAL, mortar from bedding layer	
MG12	A Pool basin	1 st Century CE First Phase	STRUCTURAL, cement core of pool steps	

Table 1: Chart of sampling context.

2.2 The Villa Draghi Quarry Site

The selected quarry site lies within the grounds of Villa Draghi, an early modern estate that rests along the western slope of Monte Alto. Originally built in the sixteenth century, it was renovated several times by its various owners to fit the styles of their respective eras. The structure and its 32-hectare plot of land have been under the jurisdiction of the Municipality of Montegrotto Terme since 1972 and are incorporated into the larger Euganean Hills Regional Park. Due to the private nature of the site, the area around Villa Draghi maintains ancient features that may have once persisted throughout the Euganean Hills. The extraction of Euganean trachyte continued into the 20th century, erasing premodern impressions on the landscape. The quarry at Villa Draghi provides a unique look into the ancient construction industry of Patavium.

Large, rectangular voids allude to the removal of blocks from the quarry. Pick marks litter the artificially vertical walls, and a sooty deposit on the roof of the cave could be related to the burning of torches in antiquity (Figure 5).

Eight samples were taken by S. Dilaria and M. Secco in 2023 (Figure 10). Samples VD03, VD04, and VD07 are ceramic finds and are not included in this study, though they may provide crucial context to understand the chronology of the quarry.

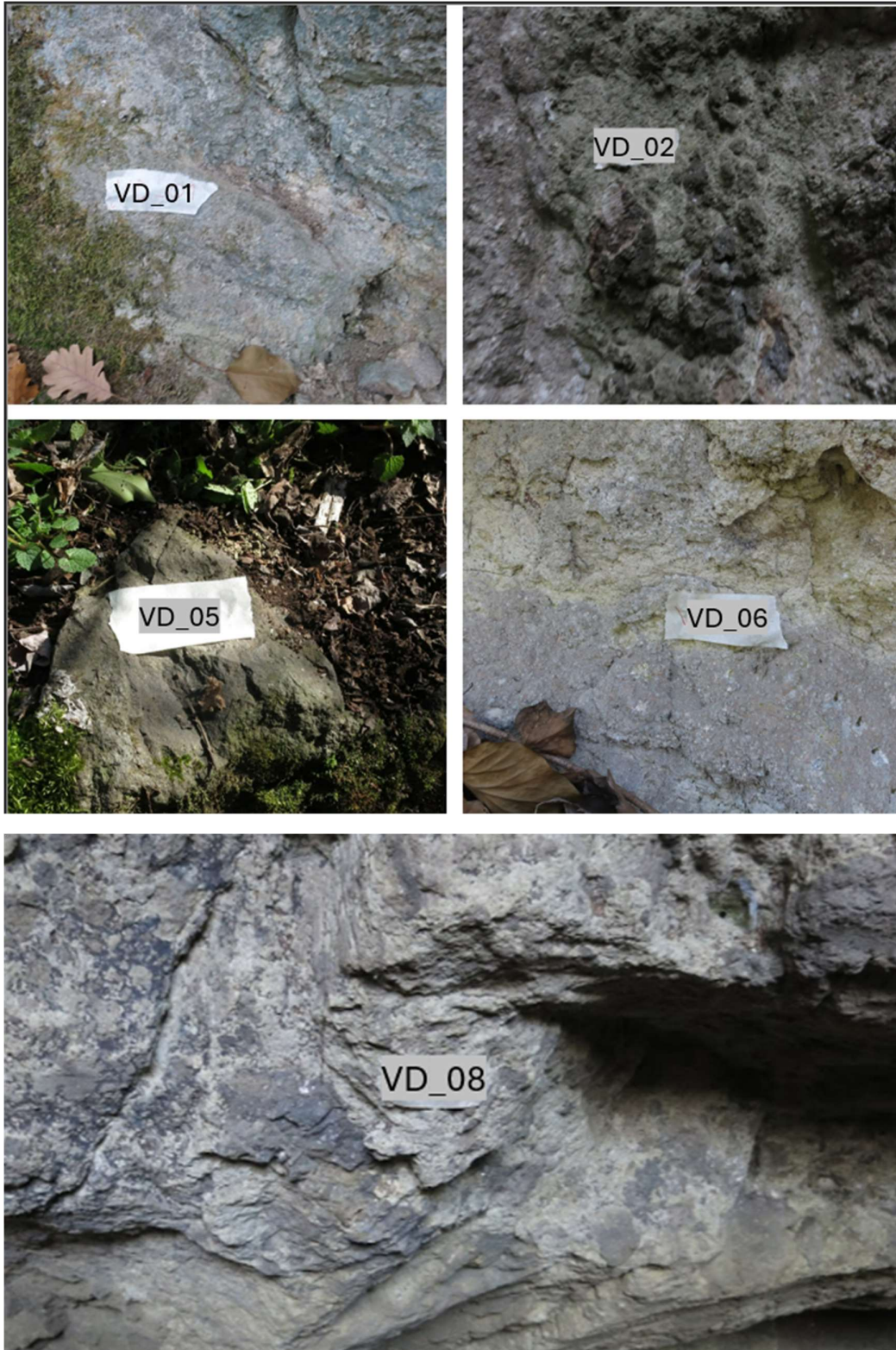


Figure 10: Sampling of Villa Draghi Quarry, photos by S. Dilaria 2023

3. Scientific Methods

A combination of qualitative and quantitative tests provided a more thorough understanding of both archaeological and geological materials. Petrographic analysis using polarized light optical microscopy (PL-OM) formed the foundation from which specific samples were selected for further geochemical and mineralogical analysis. With the hypothesis that trachytic breccia may be present in all samples, there is a strong possibility that multiple reactive aggregates were used at various phases of construction.

To evaluate the potential relationship between the archaeological site and the geological material, X-ray powder diffraction (XRPD) and x-ray fluorescence (XRF) was performed. Geochemical study was further complemented by scanning electron microscopy and energy dispersive x-ray spectroscopy (SEM-EDS).

3.1 Petrographic Analysis

Eight samples were chosen to represent the main structures of the complex in thin sections. Using a Leica DM7500 P polarized light microscope at a magnification of 1.6x and 4x, analysis showed a mineralogical diversity in aggregates and in the reaction strength amongst the various samples. Thin sections of 30 microns thickness were studied without reference to the sampling map to ensure minimal bias in grouping decisions. An integrated digital camera FLEXCAM C1 was used to capture digital micrographs of sections. All petrographic study occurred at the Department of Cultural Heritage of the University of Padova.

3.2 XRPD:

Four groups of analysis were performed using XRPD: bulk mortars, bulk geological samples, isolated geological clasts from the archeological mortars, and the separated binder fraction of the mortars. Constraints on choosing material to grind involved a selection of visibly unaltered pieces. The final weight of analysis, with added zincite standard, was approximately 1 gram. For the binder fraction, a micro-sampling of 25 milligrams was loaded on a non-diffracting sample holder.

Each bulk sample was mechanically crushed by hand or with a blunt object to millimetric size. The powder was then transferred to a mortar and ground with a pestle until approximately under 500 microns in diameter. Approximately 2 grams of powder per sample was then mixed with 15 milliliters of ethanol and inserted into a micronizing mill for five minutes. The slurry was poured onto a glass plate and allowed to dry for 24 hours. Upon drying, the powder was weighed to 0.800g and mixed with 0.200g of dehydrated zincite powder. This was again inserted into a mortar and a pestle was applied to cohesively mix the fine powders. The bulk mortar, volcanic clasts, and bulk geological powders were poured into a backloading sample holder to offset the potential preferred orientation of crystals found within the sample. The binder fraction was smeared on a zero-background microsample holder.

For effective analysis, XRPD requires grinding samples into fine powder to statistically improve the random orientation of each crystal. The x-ray is then diffracted across the various faces of each crystal, and this pattern is captured by the detector (Moropoulou et al. 1995). The patterns of most minerals and their atomic structures are defined. Analysis was performed using a Bragg–Brentano θ - θ diffractometer (PANalytical X’Pert PRO, Cu K α radiation, 40 kV and 40 mA) equipped with a real-time multiple strip (RTMS) detector (Malvern PANalytical, Malvern, UKPIXcel by Panalytical). Data was acquired by continuous scan from the angles 4–85 ($^{\circ}2\theta$) for regular samples and 4-89 ($^{\circ}2\theta$) for micro-samples with a virtual step scan of 0.02 ($^{\circ}2\theta$).

Using Malvern Panalytical’s software *HighScore Plus*, one can reference PDF databases from the International Centre for Diffraction Data (ICDD) to decipher the diffraction output and match it to known crystal lattices. Quantitative phase analysis by Rietveld refinement was performed through Bruker’s *Topas.DiffracPLUS* software, retrieving structural data from the International Crystal Structure Database (ICSD). A drawback of XRPD is that it relies on crystalline structures to reflect the x-rays from every possible crystal surface. The amorphous particles of pozzolan and C-S-H will not register, as they lack defined crystal lattices at an atomic level. However, the phenocrysts within the glassy matrix are still visible under XRPD and their mineralogy and ratios, if sufficiently diverse, would provide enough information to identify the variety and origin of breccia within the mortar samples. To account for this unmeasured fraction, the addition of zincite (ZnO) as a standard will allow the later calculation of amorphous phase percentages. In this way, one receives an indirect understanding of

the C-S-H and AFm development. A more reactive pozzolanic mortar will contain higher amorphous percentages.

Finally, XRPD data was further refined using the BGMN-Profex software, to extrapolate the quantity of disordered paracrystalline phyllosilicate gels per sample (Secco et al. 2020).

3.3 Wet Gravimetric Separation of the Binder fraction

To gain a better understanding of the components of the binder fraction, wet gravimetric separation was performed on samples MG01, MG05, and MG10. These samples were chosen due to their high percentage of amorphous content under XRPD and their abundance of material for analysis. The isolation of the binder fraction can provide insight to the production and reactivity between the mortar and aggregates (Maravelaki-Kalaitzaki et al. 2003).

Thirty grams of each sample were gently pulverized by hand and placed in a solution of ultrapure water and the anti-flocculation agent sodium hexametaphosphate (SHMP) to prevent clumping (0.5g SHMP/500ml H₂O). This mixture was set in an ultrasonic bath for 20 minutes until the binder fraction was detached from the aggregate. The suspended binder was removed via pipette and mixed again with the salt solution. The solution was agitated manually and left to settle for 24 hours, considering Stokes Law (Addis et al. 2019).

After 24 hours, the topmost portion (approximately 125ml) of each mixture was syphoned via pipette into a flask. The flasks were placed into a centrifuge and spun at 10,000 rotations per minute for 20 minutes to allow the binder to separate from the solution. The solution was later removed and replaced with ethanol to promote rapid evaporation, leaving behind only the binder in powder form on a glass plate. The samples were prepared for XRPD and SEM study.

3.4 SEM-EDS

Scanning electron microscopy and energy dispersive X-ray spectroscopy (SEM-EDS) was chosen to analyze the microstructural and microchemical characteristics of representative mortars and binder fractions.

In SEM, secondary electrons, those that are expelled from the outer shell of atoms, provide a morphological view of the analyzed object up to nanometer scale. SEM-BSE (backscattered electron) analysis meanwhile follows the beam-generated electrons, and through a sensor interprets the elastic interaction between the beam and sample by monitoring the intensity of reflected electrons. The energy dispersive spectrometer provides a partially quantifiable elemental composition of areas or selected points of the sample.

Analysis was performed with a COXEM EM-30AX Plus scanning electron microscope at the University of Padova's CEASC laboratory. It is equipped with a tungsten filament, a solid type 4-channel BSE detector, and an energy dispersive X-ray detector (EDX) EDAX Element-C2B. Samples were analyzed at various magnifications and indirect images were collected to highlight zones of interest in the mortars, particularly the reaction rims and cryptocrystalline matrices.

Selected thin sections made from the Via degli Scavi site were sputtered with a nanometric layer of graphite to induce higher electrical conductivity to optimize scanning and microanalysis. Thin sections were studied under high vacuum. Binder fraction samples were mechanically compressed into tablets. The tablets were attached to sample holder by carbon tape and received no coating to improve conductivity. Due to the fragile nature of the samples, they were studied in the low-vacuum setting.

3.5 XRF

XRF is a type of spectrometry that shows the elemental chemistry of a sample through atomic excitement. It cannot tell the relationships between elements, and therefore cannot identify a specific mineral or crystal structure from its composition. It is up to the researcher to adequately understand geological properties to match the elemental ratios to known minerals. Using the XRPD results as a guide to account for the crystalline structures, one can assign the silica and alkaline elements to their probable crystalline and amorphous configurations.

All XRF preparation took place at the Department of Geosciences at the University of Padova. Geological and archeological samples were prepared by manual grinding with mortar and pestle and dry gravimetric separation via a sieve of 180 microns. Care was taken to select unaltered portions of samples: the aggregate clasts were refined using both sandpaper and an electric sanding wheel to remove reacted

zones and any lingering binder fraction. At least 1.5 grams of material was collected per sample to facilitate a statistically relevant representation of the chemical results.

XRF was performed using a WDS Panalytical Zetium sequential spectrometer equipped with a 2.4kW Rh tube under vacuum. To measure loss of ignition (L.O.I.) the samples were calcined to 860 degrees C for 20 minutes, then increased to 980 degrees C for 2 hours inside a muffle furnace. The samples were further processed into beads using a flux of lithium tetraborate ($\text{Li}_2\text{B}_4\text{O}_7$) at a dilution ratio of 1:10. The bead was produced in a Claisse Eagon 2 bead mill at a maximum temperature of 1150 degrees C. This analysis produces a calculated percentage of major elements at an instrumental precision of 0.6%, presented as oxides (Si, Ti, Al, Fe, Mn, Mg, Ca, Na, K, and P). Trace elements (Sc, V, Cr, Co, Ni, Cu, Zn, Ga, Rb, Sr, Y, Zr, Nb, Ba, La, Ce, Nd, Pb, Th, and U) are presented in parts per million (PPM) with an instrumental precision of 3.0%.

Detection limits of major and trace elements are as follows:

Al, Mg, Na = 0.01%	Si = 0.2%	Ti, Fe, Mn, Ca, K, P = 0.005%
Sc, Co, Ni, Cu, Zn, Ga, Rb, Sr, Y, Zr, Nb, Th, U = 3 PPM		
V, Pb = 5 PPM	Cr = 6PPM	Ba, La, Ce, Nd = 10 PPM

This technique was utilized to determine the provenance of the archeological material according to geochemical compatibility of measured clasts from mortars samples and a dataset of geological samples, as commonly adopted in literature for provenance tracking of volcanic rocks (Maritan et al. 2013) (Tykot 2017) and pozzolans (Dilaria et al. 2023) (Columbu et al. 2019).

The geological reference database used for this comparison consists of samples of Euganean trachyte and rhyolite, analyzed with the same techniques (Dilaria et al. 2024) and currently stored within the in-house database developed by the Department of Cultural Heritage of the University of Padova, complimented by new samples of trachytic and rhyolitic breccias collected and analyzed within the scope of this thesis.

Provenance determination was founded on the correlation of a selection of discriminant trace elements in bivariate scatterplots between volcanic rocks collected from archaeological samples and reference geological rocks. Provenance was determined by statistical modelling based on linear discriminant analysis (LDA) that identified the best matches between geological samples of known origin and the archaeologically derived clasts using a selection of discriminant trace elements. LDA results were calculated with the software *Statgraphics Centurion 19*.

Table 2 represents the outcrops referenced for provenance calculations, including the geological samples from Villa Draghi. Actual data from these samples are the intellectual property of the University of Padova.

Outcrop	Rock Chemistry	N° of Reference Samples
Catajo	Rhyolitic Breccia, Latitic Breccia	3
Denti dea Vecia	Rhyolite	1
Forche del Diavolo	Rhyolite	3
M. Alto	Trachyte, Trachy-Rhyolite, Rhyolitic Breccia	8
M. Bello	Trachyte	7
M. Brusà	Rhyolite	3
M. Castello - Montegrotto	Trachyte, Rhyolite	5
M. Cero	Trachyte	9
M. della Madonna	Trachy-Rhyolite	1
M. Grande	Trachyte, Trachy-Rhyolite	8
M. Lispida	Trachyte	3
M. Lonzina	Trachyte	3
M. Lozzo	Trachyte	6
M. Marco	Trachytic Breccia, Basaltic Trachyandesite (Breccia)	3
M. Merlo	Trachyte	36
M. Murale	Trachyte	5
M. Mussato	Rhyolitic Breccia	1
M. Oliveto	Trachyte, Rhyolite, Trachy-Rhyolite	43
M. Orsara	Trachytic Breccia	1
M. Ortone (RhY)	Rhyolite	2
M. Pigozzo	Rhyolitic Breccia	1
M. Ricco S (Rhy)	Rhyolite	1
M. Rosso	Trachyte	7
M. Rusta	Trachy-Rhyolite, Trachyte	8
M. San Daniele	Trachyte, Trachy-Rhyolite	18
M. Sengiari	Trachyte	1
M. Solone	Rhyolite	3
M. Trevisan	Trachyte	2
M. Venda	Trachytic Breccia, Rhyolite	3
MCA	Rhyolite	1
Monselice	Trachyte	23
Monticello	Rhyolite	1
Rocca Pendice	Trachyte	3
Villa Draghi (Br)	Trachytic Breccia, Rhyolite	14
Zovon area	Trachyte	19

Table 2: samples within the UNIPD proprietary database of the Euganean Hills.

4. Results

4.1 Petrographic Analysis of Selected Montegrotto Samples

Petrographic analysis of mortar thin sections from the Via degli Scavi site revealed variation in both composition and reactivity between the various structures. Ultimately, the samples fell into two categories by their main pozzolanic aggregate: volcanic breccia (Group 1) and ceramic fragments (Group 2). One sample was an outlier: a primarily lime-based mortar with no pozzolanic aggregates (MG08).

SAMPLE	ORIGIN	POZZOLAN TYPE
MG01	Odeon (E)	BRECCIA
MG02	Odeon (E)	BRECCIA
MG03	Odeon (E)	BRECCIA
MG04	Odeon (E)	BRECCIA
MG05	Odeon (E)	BRECCIA
MG06	Odeon (E)	BRECCIA
MG07	Odeon (E)	BRECCIA
MG08	Alleged Nymphaeum (D)	OUTLIER - LIME
MG09	Hydraulic Channel (H)	BRECCIA
MG10	Pool Inner Lining (C)	COCCIOPESTO
MG11	Bath Outer Wall (C)	BRECCIA
MG12	Pool Inner Lining (A)	COCCIOPESTO

Table 3: Thin sections reviewed under optical microscopy and categorized by coarse aggregate.

4.1.1 GROUP 1: VOLCANIC BRECCIA-RICH MORTARS

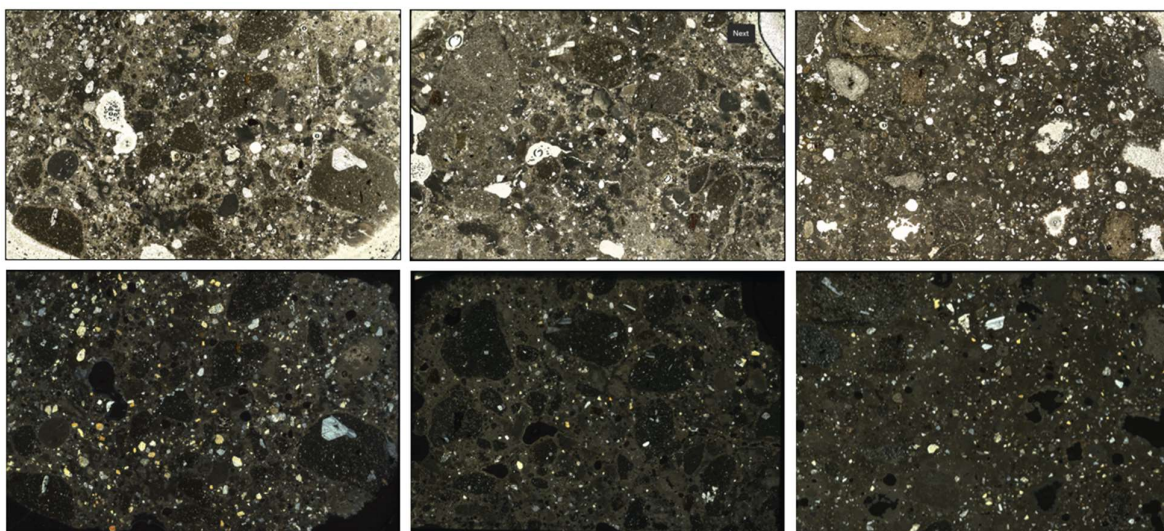


Figure 11: volcanic breccia-rich mortars (left to right: MG01, MG02, and MG04) in polarized light (PL) (top) and cross-polarized light (XPL) (bottom). These samples represent structure E. The base of each image is 3.6 cm.

Group 1 contains nine samples from three structures: MG01, MG02, MG03, MG04, MG05, MG06, MG07, MG09, and MG11. This group is distinguishable by its abundance of volcanic pozzolan within the calcic lime binder. The samples of Group 1 are characterized by a non-uniform birefringence within the micritic binder matrix; this zoning is potentially caused by variation in the distribution of hydrated phases. Lime lumps are prevalent in samples of this group apart from MG09.

Group 1 is defined by relatively low porosity with a diffused frequency of vesicles (all) and a very low frequency of vughs (MG04). Planar voids are prevalent in MG02 and MG11.

The samples present a general bimodal sorting of volcanic coarse aggregate and fine aggregate of siliceous and carbonatic sands. The clast sizes vary from millimetric to a centimeter in length. While the majority of sand clasts are rounded, the volcanic clasts are quite angular and usually coarser. This may allude to the mechanical fragmentation of trachyte and breccias at the point of extraction or may have resulted from the reuse of discarded trachyte chips from other construction projects (Figure 12). Overall, the fine and coarse aggregates are well mixed with an even distribution throughout the matrix.

Regarding mineralogy of the aggregate fraction, the sands are composed of clasts of quartz, quartzite, and chert. Few fine sands of micritic limestones and dolostones are present in Group 1. A subordinate fraction of ceramic fragments was

identified within MG02 (Figure 13). Only MG11 contains a higher percentage of fine quartzite, chert, and dolomitic aggregate that is less mixed. Some carbonate aggregates, particularly those dolomitic in nature, present evident reaction edges stemming from de-dolomitization phenomena (Katayama 2010).

The volcanic component included in Group 1 mortars is constituted by a mix of volcanic breccias from explosive diatremes (Cucato 2011) and trachyte flakes. These two types can be partially differentiated under optical microscopy by their microtexture, which reveals petro-mineralogical characteristics compatible with Euganean volcanic rocks (Capedri et al. 2003)(Dilaria et al 2024)(Germinario et al 2017)(Le Bas and Streckeisen 1991). From Figure 13, one can characterize a clast of volcanic material with crystalline groundmass and large to medium phenocrysts as porphyritic breccia, whereas those displaying an abundance of microliths within the groundmass are trachyte. This is strongly supported by the presence of sanidine phenocrysts and a glomero-cumuloporphyritic groundmass which is indicative of Euganean trachyte (Figure 10, right clast).

This volcanic component can be distinguished from clasts of Euganean breccias (on the left in Figure 10) which contain a characteristic hypocrySTALLINE to cryptocrystalline ground mass, with large to medium phenocrysts. In detail, the volcanic breccias (micrographs on the left) present a porphyritic texture and in order of abundance: phenocrysts of plagioclase (sometimes in glomerophyrs), brown amphibole (potentially kaersutite), and biotite, with a discontinuous distribution and low porphyritic index (~20%). The accessory component consists of opaque minerals and apatite. The matrix is generally hypocrySTALLINE and characterized by plagioclase microliths with a predominantly felty texture, with sporadic iso-orientations along the edges of the phenocrysts. However, distinct microstructural elements with the same mineralogical composition yet slightly different matrix characteristics are observed: vacuolar, glassy to microcrystalline in one case, and finer grained (from cryptocrystalline to microcrystalline), essentially holocrystalline in the other.

Breccia clasts tend to have a more robust reaction rim as they are more reactive within the mortar than a trachyte due to their relevant amorphous content. MG02 and MG04 present both types of volcanic material, while the remaining ones present a higher concentration of volcanic breccias.

The majority of samples present fat binder matrix to aggregate ratios, some as high as 2:1. MG09 is the leanest mortar at a ratio of about 1:1. MG04 is a very fat mortar, highlighting the diversity of ratios between aggregate and binder matrix.

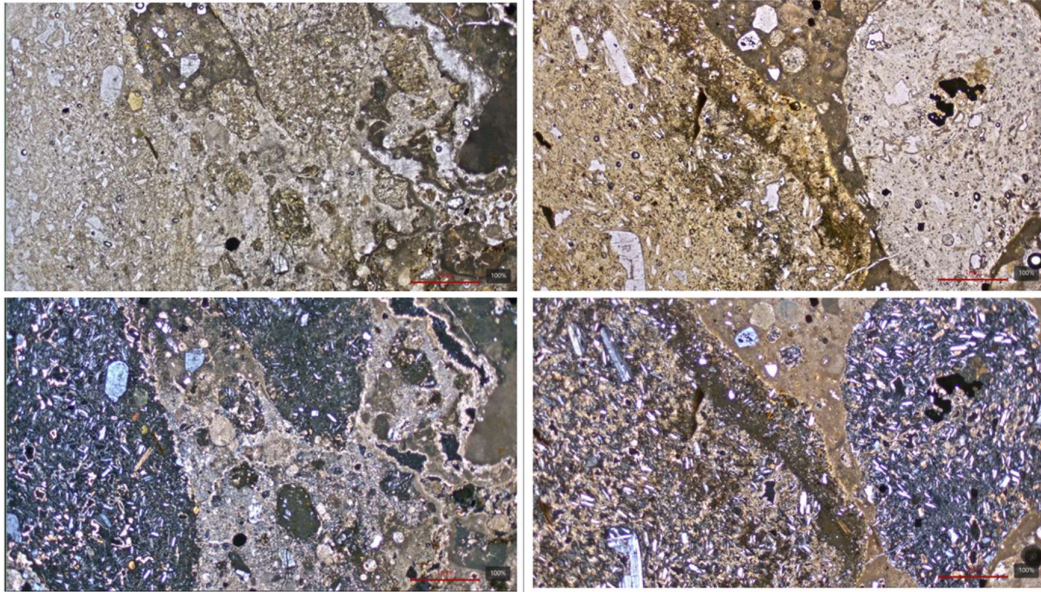


Figure 12: MG02 (left) and MG04 (right) under PL (top) and XPL (bottom). In XPL, the distinction between trachyte and trachytic breccia is clear. The trachyte groundmass has a high degree of crystallinity and a lesser amorphous component, limiting its potential reactivity with the lime binder. In contrast, breccias present a crypto-crystalline, amorphous groundmass that greatly influences its potential reaction with lime binder. Phenocrysts are primarily constituted by plagioclases (sometimes agglomerated in glomerophyrs).

Most of Group 1 samples originate from the Odeon, Structure E; this follows Roman architectural standards, as the foundation of a large structure was often made of *opus caementicium*. MG09 was sampled within the hydraulic infrastructure at structure H, and MG11 comes from an external structural wall of Pool C.

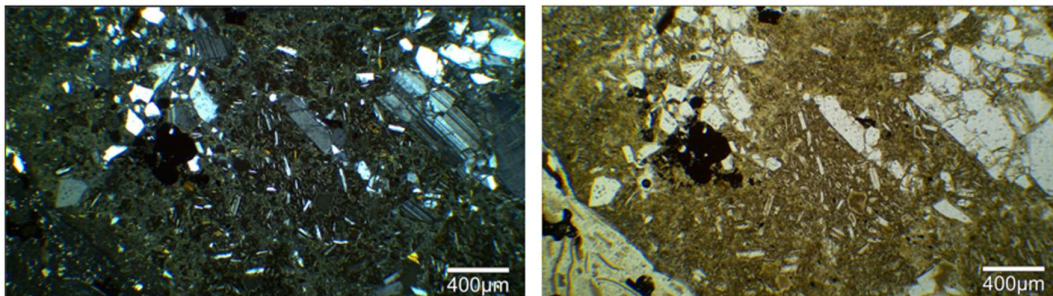


Figure 13: breccia clast from MG09 in XPL (left) and PL (right).

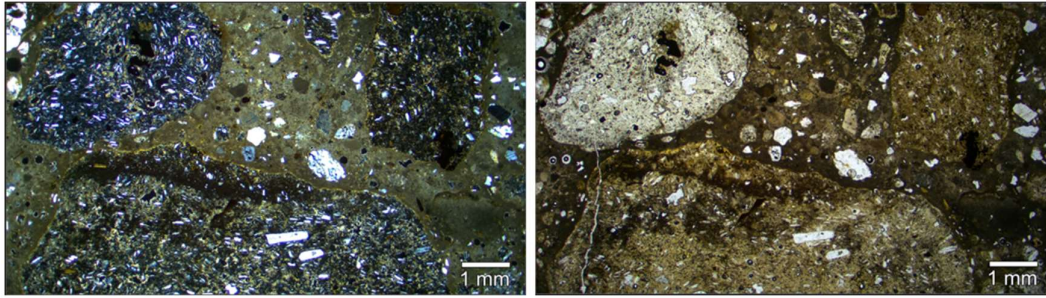


Figure 14: MG04. Left: Volcanic aggregate under XPL. The aggregate shows thin phenocrysts of alkali feldspars (white, brown) and a large opaque mineral with high metallic content (black). A visible discoloration of the surrounding binder matrix represents the reaction rim of C-S-H production. Circular voids in the matrix are lined with crystalline calcite. Right: Volcanic aggregate in PL. The angularity of the top right aggregate may hint to intentional crushing of trachyte, to be confirmed in later geochemical analysis of aggregate clasts.

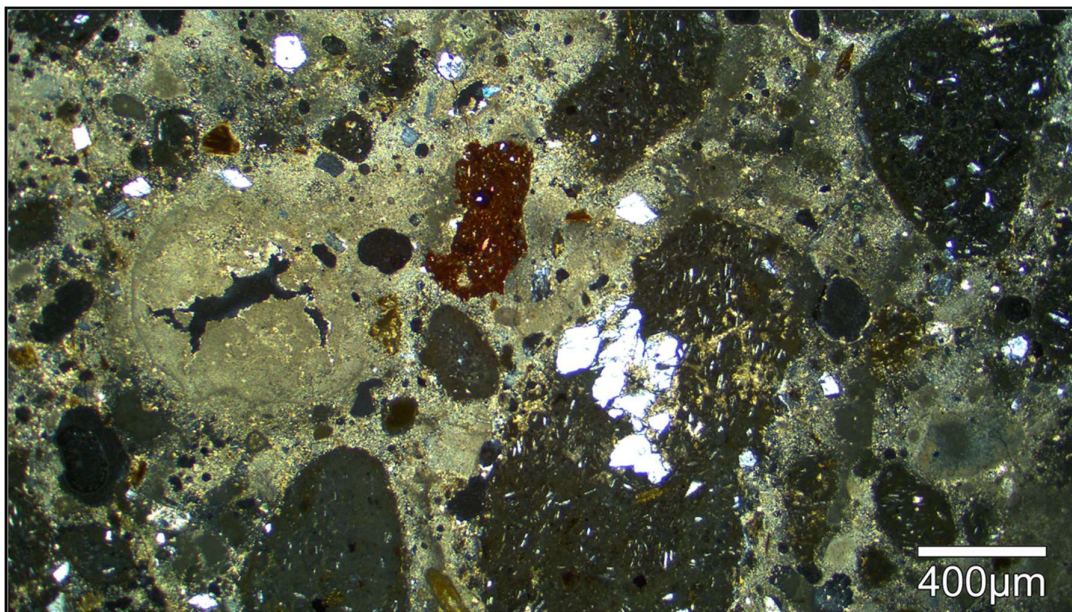


Figure 15: MG02 under XPL, depicting breccia and ceramic aggregate within a fat micritic binder.

4.1.2 GROUP 2: COCCIOPESTO-RICH MORTARS

Samples MG10 and MG12 are characterized by the abundant use of ceramic fragments as a poorly sorted coarse aggregate. The binder presents high heterogeneous birefringence to low birefringence colors; it has zones of sparry texture and others that are highly micritic. There are very few lime lumps present in this group, but they contain some limestone relics that may signify that the lime batch was not fired to an adequately high temperature. MG10 has millimetric channels and larger vughs. Vesicles are low in frequency.

A prominent feature of Group 2 is the abundance of precipitated prismatic calcite crystals along the voids within the matrix, at times filling the voids entirely,

representing newformed calcite produced from the prolonged exposure to the circulation of fluids (Pecchioni et al. 2014). The secondary calcite is explained by the origin of the samples: Group 2 contains samples from the thermal pools which experienced perpetual excess water flowing over the system. This water percolated through the pores of the binder and caused the dissolution of calcite that reprecipitated within the voids. The shrinkage of the binder during setting would create diffused planar voids. There are both planar and channel voids present, now entirely filled with calcite (Figure 16).

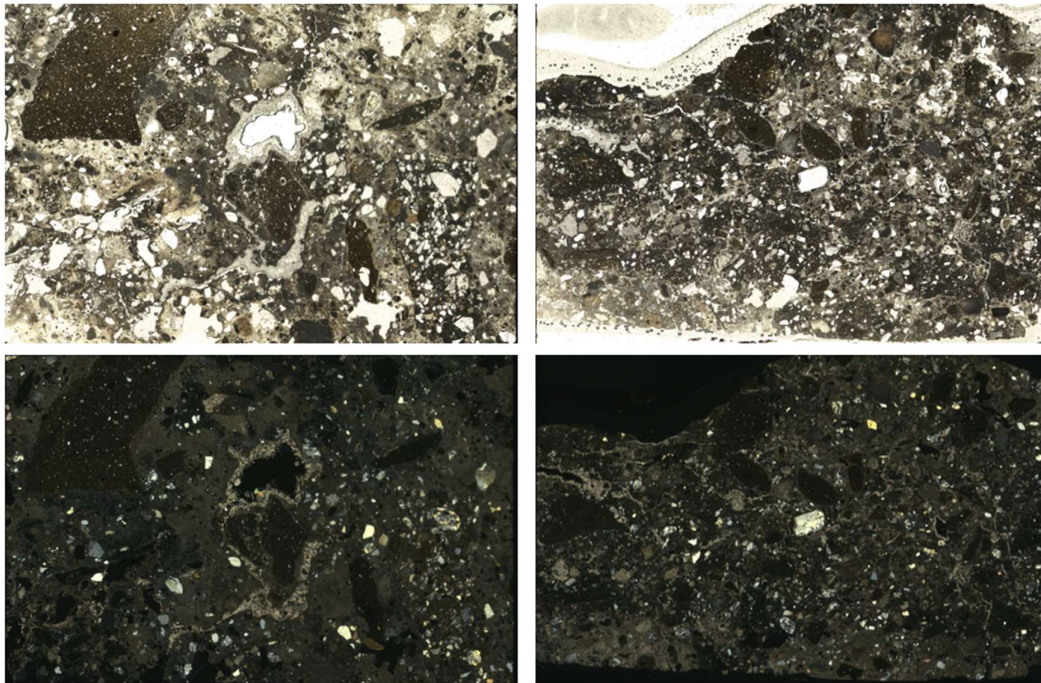


Figure 16: Sample MG10 (left) and MG12 (right) under PL (top) and XPL (bottom). The base of each figure measures 3.6 cm.

Coarse fragments of centimetric ceramic represent the largest aggregates of Group 2. MG10 is poorly mixed, with a fatter composition and fewer aggregates than MG12. MG12 presents smaller aggregates that allude to a different sorting technique and better mixing. No evidence of volcanic breccia aggregate was found in these sections. There are heavily reacted aggregates not yet identified that may be dolomitic or various carbonatic sands of subordinate quantity. MG10 contains subordinate clasts of mortar reused as aggregate, distinguishable by its heterogeneous aggregate and a higher birefringence color within its matrix (Figure 15, right). These samples present a higher concentration of well sorted fluvial sand aggregate used in comparison to Group 1 but are still relatively fat mortars with an estimated binder-aggregate ratio of 1.5:1.

As the Romans were aware of the waterproofing characteristics of ceramics when mixed with lime binders (Bonetto and Dilaria 2021), it is no surprise that these two samples originate from the thermal basins A and C. For the bath structures, builders may have chosen the conservative choice of utilizing a more broadly applied technology to ensure waterproofing.

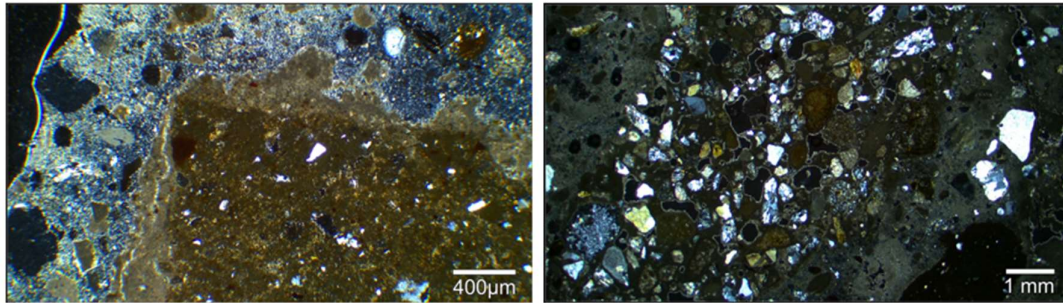


Figure 17: MG10 under XPL. Left: the thick reaction rim (light brown) surrounding the ceramic fragment suggests a high concentration of a hydrated silicate phase. Right: the central, darker matrix with higher fine aggregate is a clast of mortar that has been reused as an aggregate.

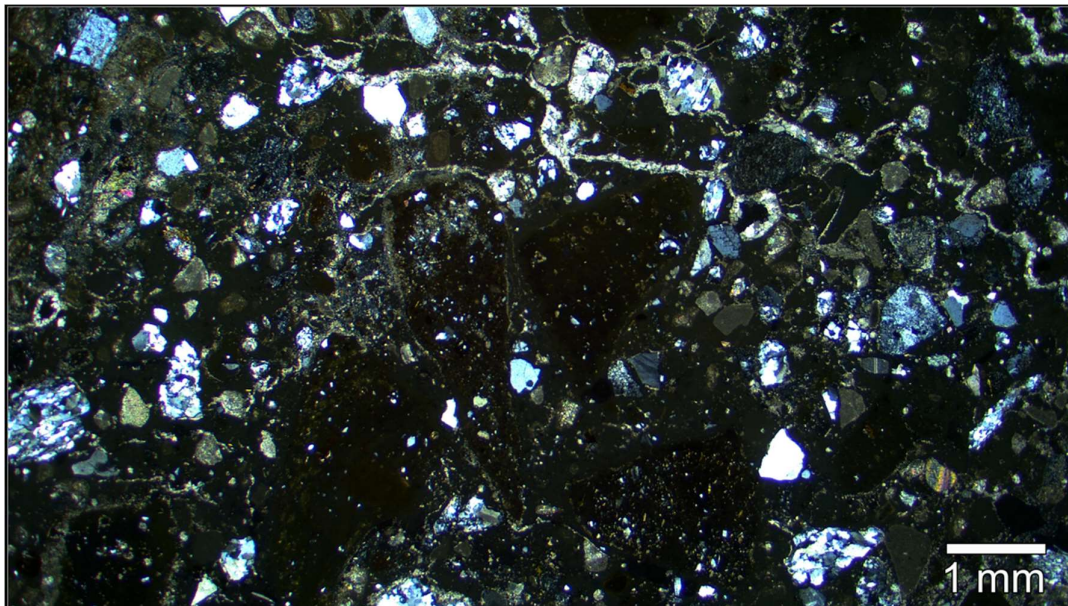
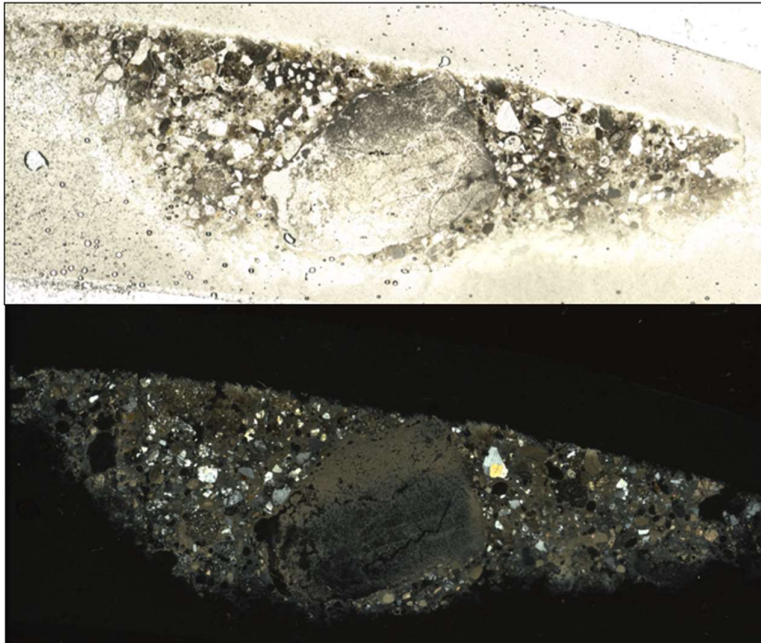


Figure 18: Sample MG12 under XPL. The capillary pores are filled with crystalline calcite. Abundant fine sands of quartzite and chert contrast the coarser ceramic fragments.

4.1.3 OUTLIER: AERIAL LIME BINDER



MG08 is the sole outlier of this study, collected from Structure D. It is a strangely cut thin section, likely due to the physical characteristics of the mortar that buckled during the mechanical extraction and resin

saturation process. Its matrix is micritic to micro-sparitic with non-uniform birefringence possibly due to a varying thickness of the section as parts fall under 30 microns. MG08 presents an abundance of centimetric lime lumps which can be distinguished in the darker birefringence clumps. MG08 is quite porous, with a high concentration of vesicles and vughs, alluding to the oversaturation of water at the time of mixing. It is characterized by a mixed presence of sparse millimetric ceramic fragments and many coarse breccia aggregates. A subordinate quantity of quartz, quartzite, and carbonatic clasts are poorly mixed in the binder. Very scattered chlorites and small presence of volcanic rocks are detectible. Chert is scarce. For this group, the volcanic material does not seem to be the reactive element, and much of the reaction may have been that of an aerial lime binder.

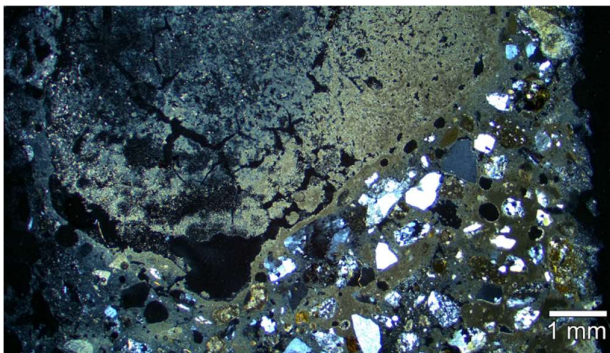


Figure 19, above: MG08 thin section in PL and XPL. The base of each figure measures 3.6 cm

Figure 20, left: Sample MG08 under XPL. Three terracotta fragments are visible (upper and center right), alongside plentiful quartzite sands and a very large lime lump (top left).

4.2 XRPD:

In total, 23 archeological samples were studied: 12 bulk mortars, 3 binder fractions, and 8 selected mortar aggregates. Eight geological samples from the Villa Draghi quarry were studied to facilitate a quantitative comparison to the mortar aggregates. The mineralogical constituents were identified and quantified as weight percentages of the total sample, using *High Score Plus* for qualitative analysis, Bruker's *Topas.DifffracPLUS* for quantitative phase analysis, and BGMN-Profex for the quantification of paracrystalline phyllosilicate gels.

4.2.1 Bulk Mortars

Sample	CAL	ARG	VT	MC	DL	QTZ	AND	OLG	ANR	SN	MSC	BIO	CLNO	DIO	HNB	HMT	MGT	ANC	ILM	PS Gels	Amorph
MG01	24.99	0.00	0.57	3.73	0.63	10.76	8.79	0.00	6.35	3.18	0.89	1.32	1.39	0.00	0.23	0.00	0.00	0.00	0.53	6.33	30.32
MG02	34.87	0.00	0.00	4.88	1.05	18.32	9.36	0.00	0.00	2.26	4.03	0.93	2.08	0.00	0.00	0.00	0.00	0.00	0.00	1.50	20.71
MG03	28.00	0.00	0.00	3.31	0.63	11.18	10.82	0.00	6.09	1.94	0.43	0.80	1.10	0.00	0.62	0.00	0.74	0.00	0.83	1.69	31.83
MG04	36.62	0.00	0.00	0.54	1.86	5.47	13.90	0.00	8.87	5.34	1.69	1.60	0.45	0.00	1.71	0.77	0.78	0.00	0.45	4.71	15.25
MG05	32.00	0.32	2.08	5.32	0.00	10.11	5.30	0.00	4.54	0.98	1.59	1.07	0.70	0.00	1.91	0.00	0.47	0.00	0.57	0.00	33.00
MG06	34.44	0.00	0.19	4.56	0.00	10.46	5.35	0.00	5.67	2.10	0.87	1.23	1.41	0.00	0.00	0.00	0.53	0.00	0.68	0.00	32.51
MG07	28.08	0.00	0.45	3.04	1.97	13.20	10.72	0.00	6.97	2.55	1.13	1.49	1.58	0.00	1.61	0.00	0.79	0.00	0.77	0.00	25.66
MG08	32.99	0.00	0.00	0.00	1.66	25.33	2.29	3.97	0.35	1.38	1.20	0.70	3.50	0.00	0.00	0.00	0.00	0.00	0.00	5.84	19.02
MG09	28.12	0.00	0.00	0.00	4.04	14.24	7.81	0.00	4.42	1.16	1.50	1.45	2.49	0.00	0.71	0.00	0.85	0.00	0.62	10.00	22.61
MG10	42.62	0.00	0.00	0.00	0.39	10.04	0.00	3.42	0.00	0.00	1.16	0.00	3.99	4.05	0.00	0.69	0.00	0.00	0.63	14.04	17.83
MG11	20.99	0.00	0.00	1.39	1.03	13.00	16.29	0.00	1.00	6.62	0.58	1.08	3.62	0.00	1.79	0.00	0.41	0.00	0.00	18.25	13.96
MG12	31.94	0.54	0.00	0.00	3.77	10.25	0.00	4.14	0.00	0.00	0.00	0.84	0.43	8.41	0.00	0.52	0.00	0.44	0.00	17.54	17.83

Table 4: Mineralogical composition of bulk mortar samples from XRPD analysis. Amorph=amorphous, CAL=calcite, ARG=aragonite, VT=vaterite, MC=monocarbonate, DL=dolomite, QTZ=quartz, AND=andesine, OLG=Oligoclase, ANR=anorthoclase, SN=sanidine, MSC=muscovite, BIO=biotite, CLNO=clinoclone, DIO=diopside, HNB=hornblende, HMT=hematite, MGT=magnetite, ANC=analcime, ILM=ilmenite, PS Gels=phyllosilicate gels

From these results, the variations in reactivity and aggregate characteristics documented during optical microscopy is confirmed. The breccia-rich mortars of Group 1 consistently contained sanidine, andesine, and anorthoclase. These minerals were dominant phases within the Villa Draghi quarry samples. Quartz varied between 10 and 18% within the bulk samples from the *odeon*. Ilmenite and magnetite were present in the majority of breccia-rich samples, though only magnetite is present in the XRPD results of Villa Draghi. Biotite and muscovite are present in all Group 1 mortars, but only biotite is detected in the VD samples. The amorphous phase varies drastically within Group 1, from MG04 at 15% to MG05 at 33%. Calcite levels vary from 20% (MG11) to 36% (MG04), with some samples containing low quantities of the polymorphs aragonite (MG05) and vaterite (MG01, MG05, MG06, MG07).

Regarding Group 2, MG10 and MG12 are the only samples containing the mineral diopside ($\text{CaMgSi}_2\text{O}_6$), typical high temperature product derived from the

carbonate-rich clay that was the base of the ceramic fragments used as coarse aggregate. MG10's makeup of 17% amorphous and 42% calcite further suggests that the calcium had leached from C-S-H and magnesium replaced it. Montmorillonite $((\text{Na,Ca})_{0.33}(\text{Al,Mg})_2(\text{Si}_4\text{O}_{10})(\text{OH})_2 \cdot n\text{H}_2\text{O})$ or hydrotalcite $(\text{Mg}_6\text{Al}_2\text{CO}_3(\text{OH})_{16} \cdot 4\text{H}_2\text{O})$ are possible Mg-rich phases that could contribute to the Mg in the system. However, it is likely attributing the significant fraction of phyllosilicate gels detected in the sample (over 14%) to a relevant occurrence of M-S-H, which has preferential formation over C-S-H in low pH environments (Kim et al. 2022). The infiltration of thermal waters activated the M-S-H precipitation, which in turn lowered the pH of the system, further inducing the dissolution of C-S-H and the precipitation of crystalline calcite.

The outlier MG08 presented the highest quartz content of all mortar samples at over 25%. Its calcite content was measured at about 33%, and the amorphous phase was calculated to be around 19%. The characteristic minerals associated with the volcanic breccia-rich mortars (ilmenite, magnesite, hornblende, monocarbonate) and ceramic-rich mortars (diopside, hematite) were not present in a perceivable quantity. Quartzite sands and lime lumps are the prevalent mineralogical features and large pores hint to the oversaturation of water during the mixing process. MG08 contains oligoclase, further diverging from the breccia-rich mortars.

4.2.2 Volcanic Aggregates & Geological Samples

Sample	CAL	VAT	MC	DL	QTZ	CRY	AND	ANR	SN	MSC	BIO	CLNO	HNB	MGT	TRD	GPS	PS Gels	Amorph
MG01_C1	3.00	0.00	0.00	0.00	4.35	0.00	15.74	11.80	4.77	0.00	2.67	0.00	1.14	1.02	0.00	0.00	6.50	49.02
MG02_C1	9.83	0.00	0.00	6.99	14.60	0.00	3.17	0.72	1.73	18.95	0.96	5.19	2.90	1.00	0.00	0.00	0.00	33.93
MG02_C3	1.59	0.00	0.00	0.00	4.79	0.00	28.93	21.91	14.56	0.00	4.01	0.00	2.17	1.81	0.00	0.00	7.50	12.75
MG03_C1	0.59	0.00	0.00	0.00	1.04	0.00	31.28	2.28	14.42	0.00	2.40	0.00	2.11	0.86	0.00	0.00	7.73	37.30
MG03_C5	2.69	0.00	0.00	0.00	0.80	0.00	35.33	2.00	21.47	0.00	1.73	0.00	2.48	0.62	0.00	0.00	9.77	23.12
MG05_C5	2.30	4.65	0.29	0.00	0.57	0.00	25.09	2.94	21.31	0.00	1.91	0.00	1.16	1.06	0.00	0.00	5.30	33.44
MG09_C1	0.30	0.00	0.00	0.00	0.88	0.00	22.88	19.26	17.24	0.00	2.09	0.00	1.50	1.45	0.00	0.00	20.60	13.82
MG09_C4	0.00	0.00	0.00	0.00	1.12	0.00	24.63	24.53	18.72	0.00	2.60	0.00	0.80	1.03	0.00	0.00	13.88	12.69
VD01_C1	0.00	0.00	0.00	0.00	0.46	0.00	28.13	2.67	8.34	0.00	2.03	0.00	1.70	1.05	0.00	0.00	26.32	29.30
VD01_M	0.00	0.00	0.00	0.00	0.69	0.00	12.22	13.06	3.94	0.00	1.25	0.00	1.12	1.23	0.00	0.00	18.10	48.38
VD02_M	0.00	0.00	0.00	0.00	1.27	0.00	13.64	14.21	3.98	0.00	1.94	0.00	1.77	2.02	0.00	0.00	12.85	48.31
VD02_C1	0.00	0.00	0.00	0.00	0.18	0.00	28.71	4.17	9.62	0.00	1.83	0.00	0.87	0.69	0.00	0.00	12.33	41.61
VD02_C2	0.00	0.00	0.00	0.00	0.60	0.00	31.26	1.89	9.66	0.00	1.94	0.00	1.52	0.99	0.00	1.18	17.83	33.16
VD05	0.00	0.00	0.00	0.00	0.76	14.32	17.77	21.85	15.77	0.00	1.82	0.00	1.96	1.90	9.57	0.00	0.00	14.28
VD06_BL	0.00	0.00	0.00	0.00	0.72	0.00	25.12	19.64	8.62	0.00	1.78	0.00	0.56	1.73	0.00	0.00	30.36	11.47
VD06_L	0.00	0.00	0.00	0.00	2.18	13.23	24.50	22.69	12.23	0.00	1.15	0.00	3.38	0.00	9.26	0.00	0.00	11.39
VD06_WB	0.00	0.00	0.00	0.00	0.63	0.00	24.98	20.14	11.09	0.00	2.09	0.00	0.84	1.76	0.00	0.00	27.33	11.16
VD08	0.00	0.00	0.00	0.00	0.93	0.00	16.03	13.41	4.87	0.00	1.59	0.00	1.92	1.83	0.00	0.00	12.19	47.24

Table 5: XRPD results for archaeological clasts and geological samples. CAL=calcite, VT=vaterite, MC=monocarbonate, DL=dolomite, QTZ=quartz, CRY=cristobalite, AND=andesine, ANR=anorthoclase, SN=sanidine, MSC=muscovite, BIO=biotite, CLNO=clinochlore, HNB=hornblende, MGT=magnetite, TRD= tridymite, GPS=gypsum, PS Gels=phyllosilicate gels, Amorph=amorphous.

The MG volcanic clasts have residual calcite, vaterite, and monocarbonate from the intrusion of binder within the pores of the clasts. Due to the reactions within the mortar, the clasts are altered from their original geochemistry and therefore cannot be truly identical to the samples recently collected from the geological setting. However, similar mineralogical trends give evidence of geological relation. VD samples are highly correspondent with MG clasts in levels of andesine, anorthoclase, sanidine, biotite, hornblende, and magnetite.

The bulk sample was very friable and could be crushed by hand to release the clasts. This ease of access would make it a valuable commodity as it would require less intensive labor during extraction. VD05 and VD06_L contain cristobalite, a high-temperature polymorph of quartz; the two samples certainly formed at higher temperatures.

MG03_C1, MG09_C1, and MG09_C4 contain little to no calcite, so they may represent the least altered archeological clasts. VD01_C1, VD02_C1, and VD02_C2 are geologically sourced clasts manually removed from a larger bulk sample. VD08 contains a very high amorphous content (47.24%), as do the bulk samples of VD01_M (48.38%) and VD02_M (48.31%). The XRPD results provide a strong reference to the variations in mineralogy of both the quarry and the volcanic aggregates. However, it is not enough to determine the precise provenance of the archeological samples.

4.3 SEM-EDS

Samples MG02 and MG11 were chosen to represent the breccia-rich mortars of Group 1. Both ceramic-rich mortars MG10 and MG12 were analyzed for Group 2. The outlier MG08 was not considered for this part of the study.

SAMPLE	Group	Structure	% Amorphous	% Calcite
MG02	1	E	20.713	34.868
MG11	1	C	13.964	20.987
MG10	2	C	17.832	42.621
MG12	2	A	17.829	31.936

Table 6: Thin Sections chosen for SEM, with indicated the weight percentages of calcite and amorphous phase calculated through Rietveld refinement from XRPD.

Several factors were studied during SEM-EDS. For each sample, a magnification of the binder fraction was attempted. The aggregates were also chemically analyzed by EDS to confirm chemistry. Most importantly, the reactive aggregates of both groups were highlighted for analysis. Both the matrix of the aggregate and the reaction rims were selected for areal EDS scans. Carbon was omitted from the following results due to the likelihood of interference from the graphite that was used in the sputter coating of the thin sections.

SEM-EDS results followed a similar trend to XRPD: it is apparent that the two groups of mortar experienced different pozzolanic reactions due to their reactive aggregate. The volcanic breccia-rich mortars of Group 1 underwent the expected C-S-H formation in interfacial zones, forcing a partial dissolution of the breccia and triggering reactivity in carbonate aggregates. Diverging completely, Group 2's ceramic-rich mortars have undergone a decalcification, if C-S-H had ever originally been the primary pozzolanic product. Group 2 samples present a high production of M-S-H, a magnesium-based alternative to C-S-H whose formation in the analyzed samples can be related to the high magnesium content within the ceramic and a strong leaching process from the percolation of water in the system.

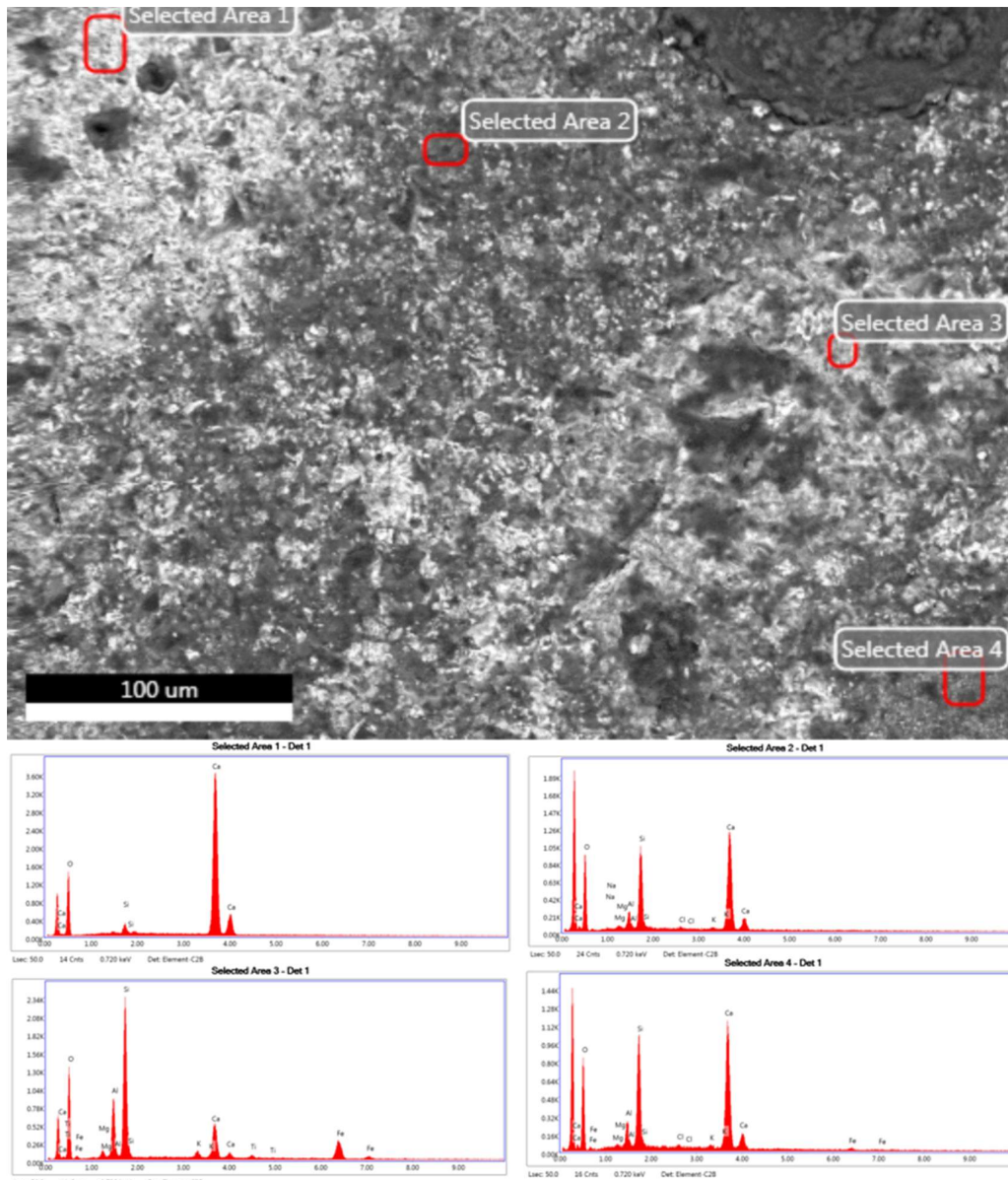


Figure 21: SEM of MG02 at 500x magnification. Areas of high pozzolanic reactivity appear within the binder matrix.

In MG02, the binder was probed to reveal microcharacteristics and chemical trends. The darker areas (2 and 4) present calcium, silica, and oxygen in equal ratio, leading to the conclusion that C-S-H is abundant in darker zones. Area 3 shows higher iron and aluminum content, likely an AFm phase or partially reacted fine pozzolanic particles. This could allude to the addition of pozzolanic powder alongside the coarse aggregate.

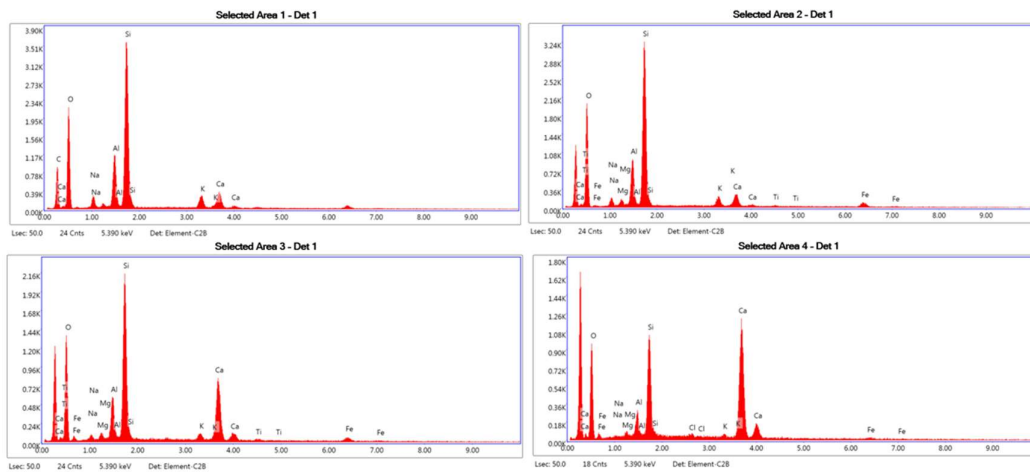
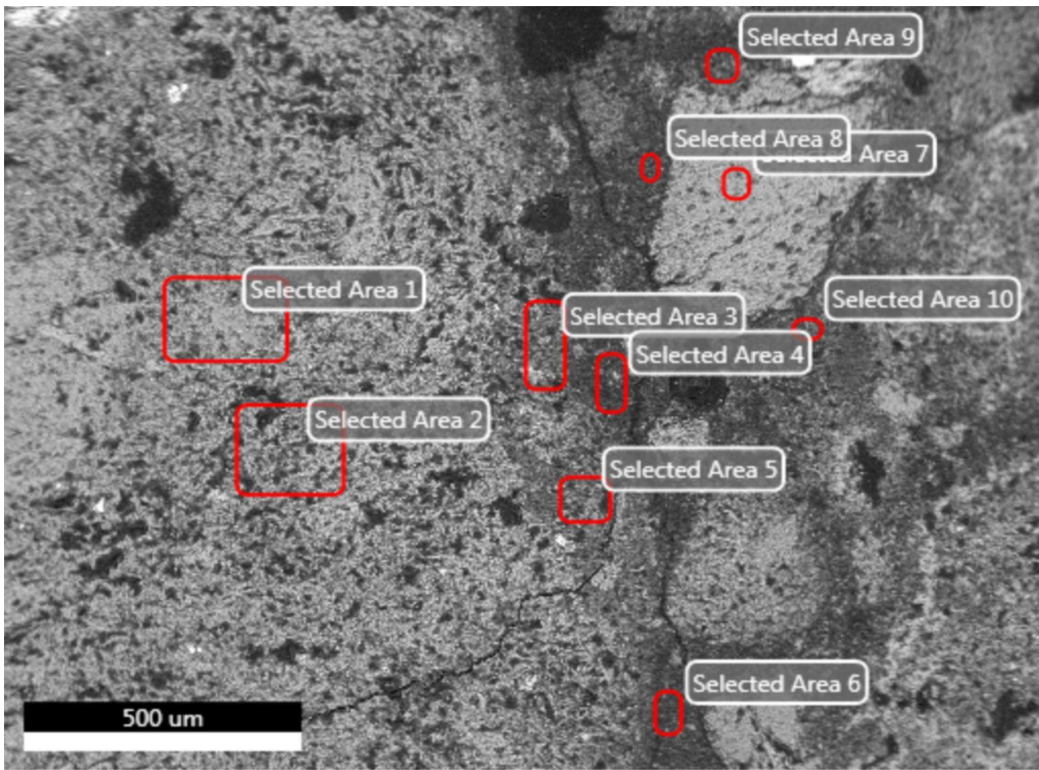


Figure 22: MG02 at 500x magnification. Areas 1 and 2 represent a breccia clast, and areas 3 and 4 are part of the reaction rim.

Within the breccia clast itself (areas 1 and 2), there is some calcium percolation. It is high in silica and aluminum, indicating strong reaction potential. As one approaches the boundary of the clast, the calcium content increases (area 3) until it is equant to the silica and oxygen (area 4). This interstitial zone is likely composed of C-S-H and some C-A-H, as aluminum content remains in a lesser percentage.

MG11

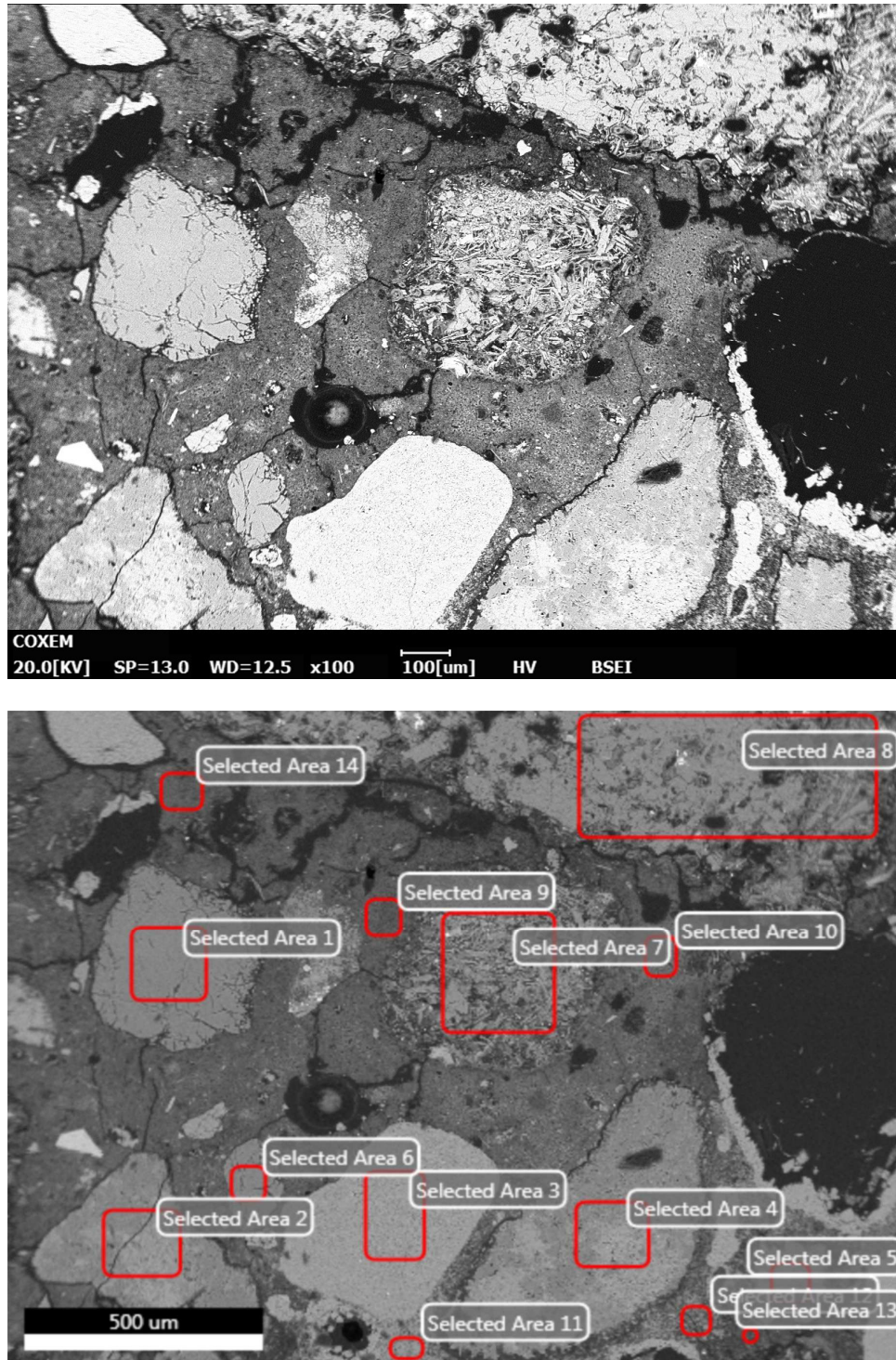


Figure 23: MG11 aggregates of siliceous and dolomitic sands as well as volcanic breccia at 100x magnification. The phenocrysts and holocrystalline matrix of the breccia aggregate are visible (area 7).

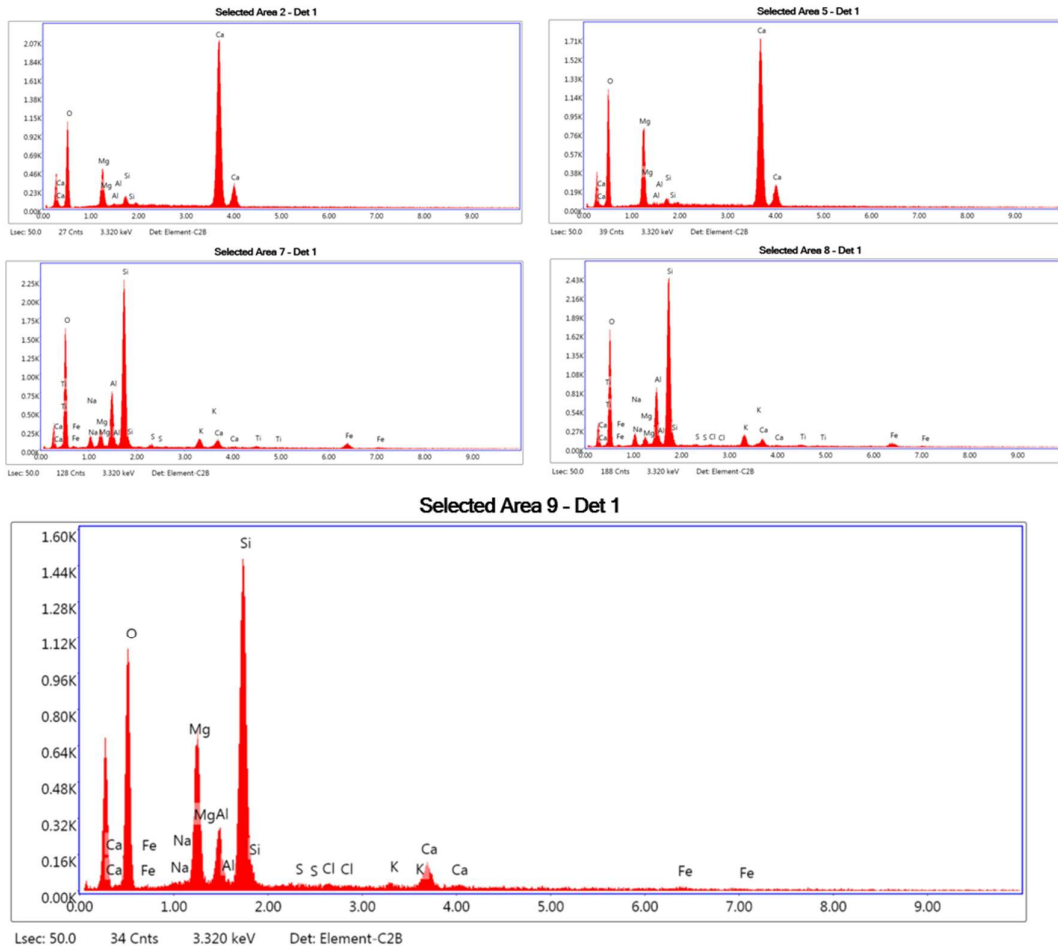


Figure 24: EDS results from area surveys of MG11 aggregates. Areas 2 and 5 appear to be dolomitic sands while areas 7 and 8 are volcanic breccia.

Dolomitic (areas 2 and 5) and siliceous sands (areas 1 and 6) accompany the breccia clasts as coarse aggregate. An equant Mg:Si:O ratio was detected in area 9 and 14, which might indicate M-S-H production in sporadic zones when Mg is available in the system. In this case, the Mg would be sourced from the dolomitic sands. Another product of dedolomitization is periclase, a magnesium oxide; however, as no crystalline periclase was detected during XRPD, it is more likely that the magnesium silicate is represented as phyllosilicate gels.

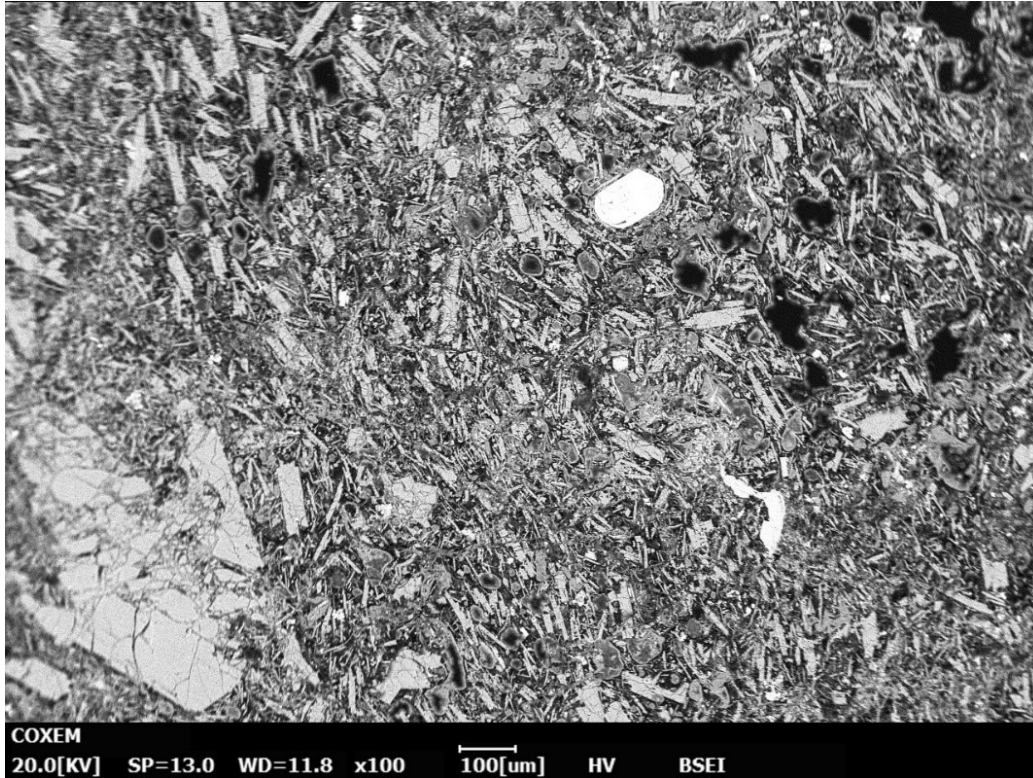


Figure 25: MG11 breccia clast at 100x magnification. Phenocrysts and pores are distinguishable due to their varying atomic weights, lighter crystals equate to heavier minerals. This breccia is dominated by aluminum-rich silicates.

The breccia matrix remains consistent to observations made during optical microscopy, with high silica, oxygen, and aluminum content relate to the occurrence of feldspars. The large plagioclase phenocryst (bottom left) has very low potassium content. The pores evident in the indirect image would allow the pozzolanic reaction to reach a wider surface area (Figure 27).

MG10

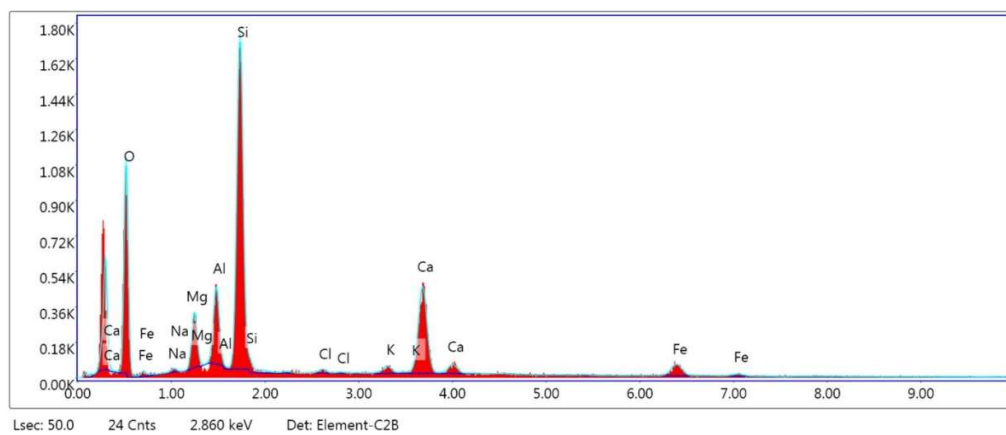
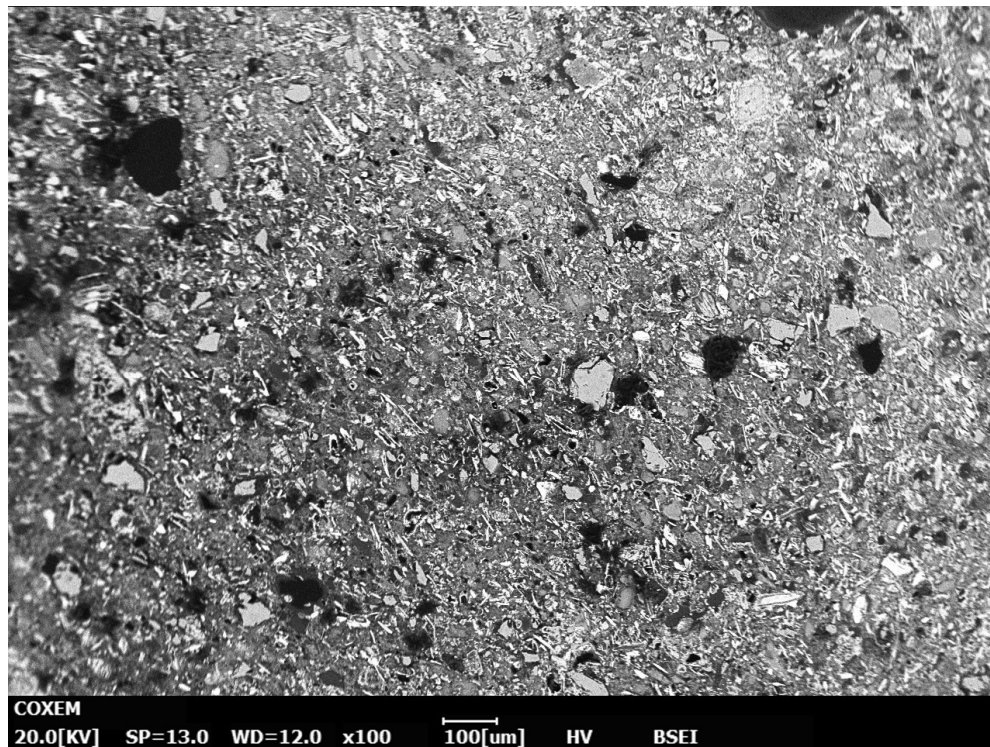


Figure 26: MG10 ceramic fragment matrix at 100x magnification and corresponding EDS chart.

The ceramic aggregates are rich in silica, magnesium, and aluminum. The high calcium content within the ceramic matrix comes from the infiltration of lime during the mortar reaction process.

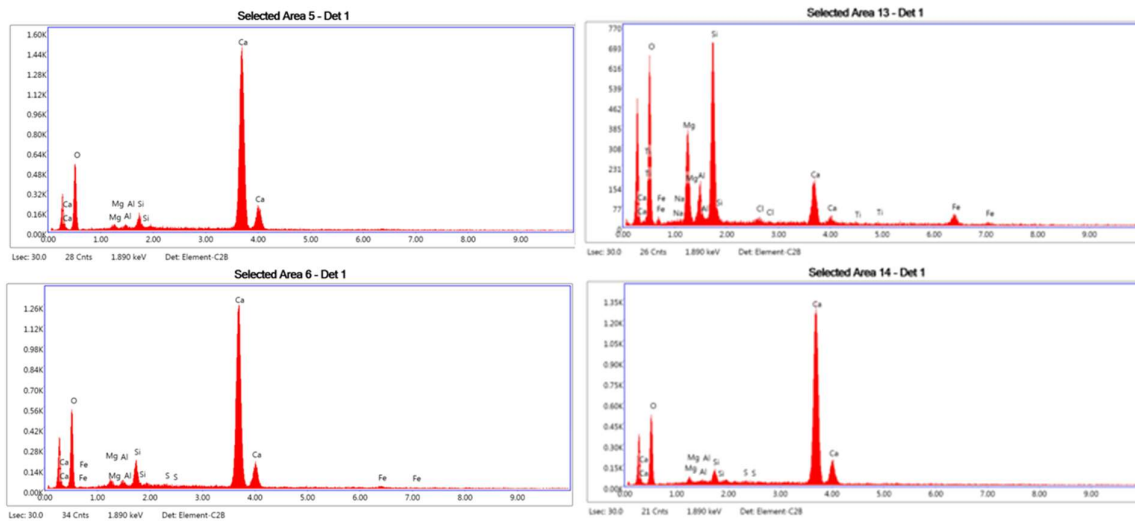
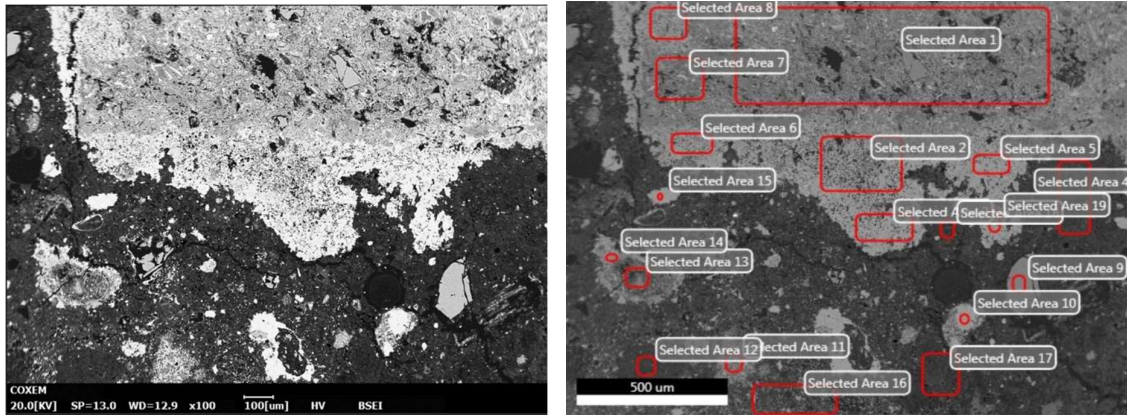


Figure 27: MG10, area with ceramic fragment and reaction rim at 100x magnification.

The ceramic-rich mortars experienced heavy inundation due to their function as sealant for the hydraulic pools. Under SEM, it is evident that the pores of the mortars had filled with reprecipitated calcite (areas 5 & 6), leached from the system by continuous water flow. However, the high amorphous content remained, even where C-S-H was low. The magnesium from the ceramic fragments appears to have been released into the system, replacing the former C-S-H with M-S-H (magnesium silicate hydrate). This allowed for the continued structural function of the mortar despite its long-term alteration. Under SEM, crystalline calcite is identifiable. Furthermore, Mg-rich carbonate sands in alkali solution will dissolve, releasing Mg and Ca into the system (Štukovnik et al 2019). This produces a carbonate halo (area 14) around the reacting aggregate (Area 13). Despite the aggregates registering approximately 15-25% Mg under SEM-EDS, the bulk mortar XRPD results reported that MG10 had under 0.40% dolomite (CaMgCO_3) and no detected brucite ($\text{Mg}(\text{OH})_2$).

MG12

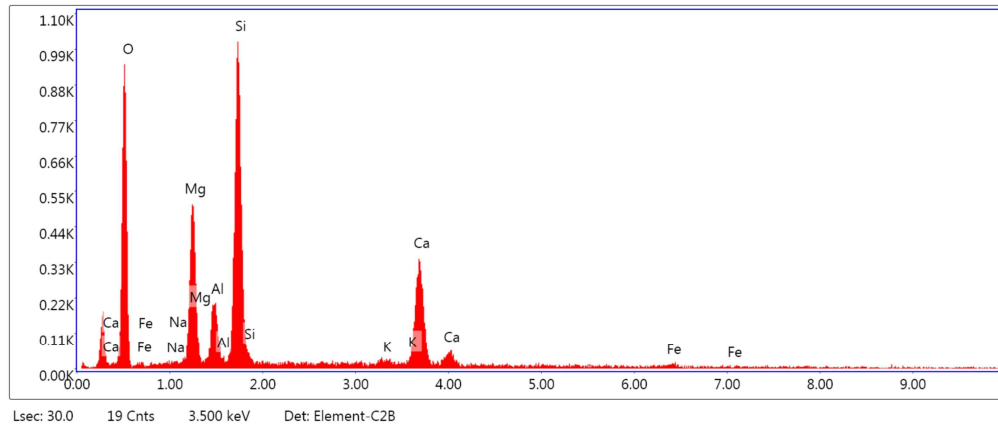
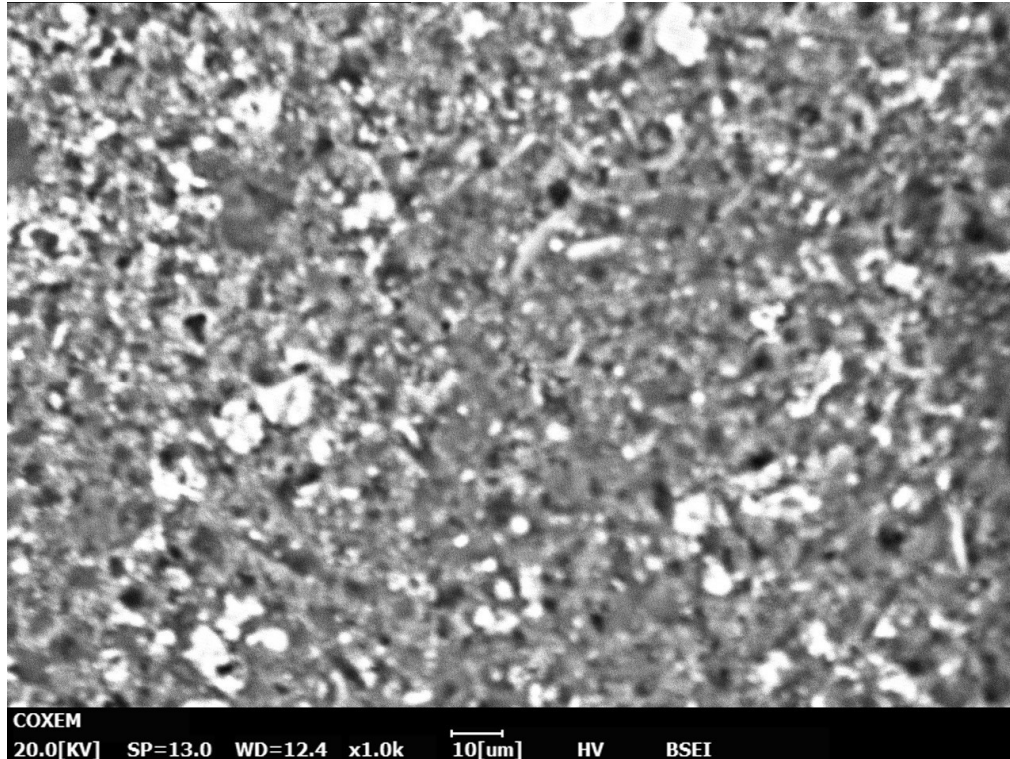


Figure 28: MG12 at 1000x magnification, focused on the binder matrix. The rate of Mg and Ca in the system allude to both M-S-H and C-S-H formation.

The binder fraction of MG12 also presents high percentages of MG, Al, and Ca. The Mg:Ca:Si ratio can be attributed to the formation of both C-S-H and M-S-H, but the calcium can also represent an aerial lime reaction that led to the formation of calcite. MG12 had no monocarbonate registered by XRPD, but it may have formed an M-A-H equivalent of C-A-H.

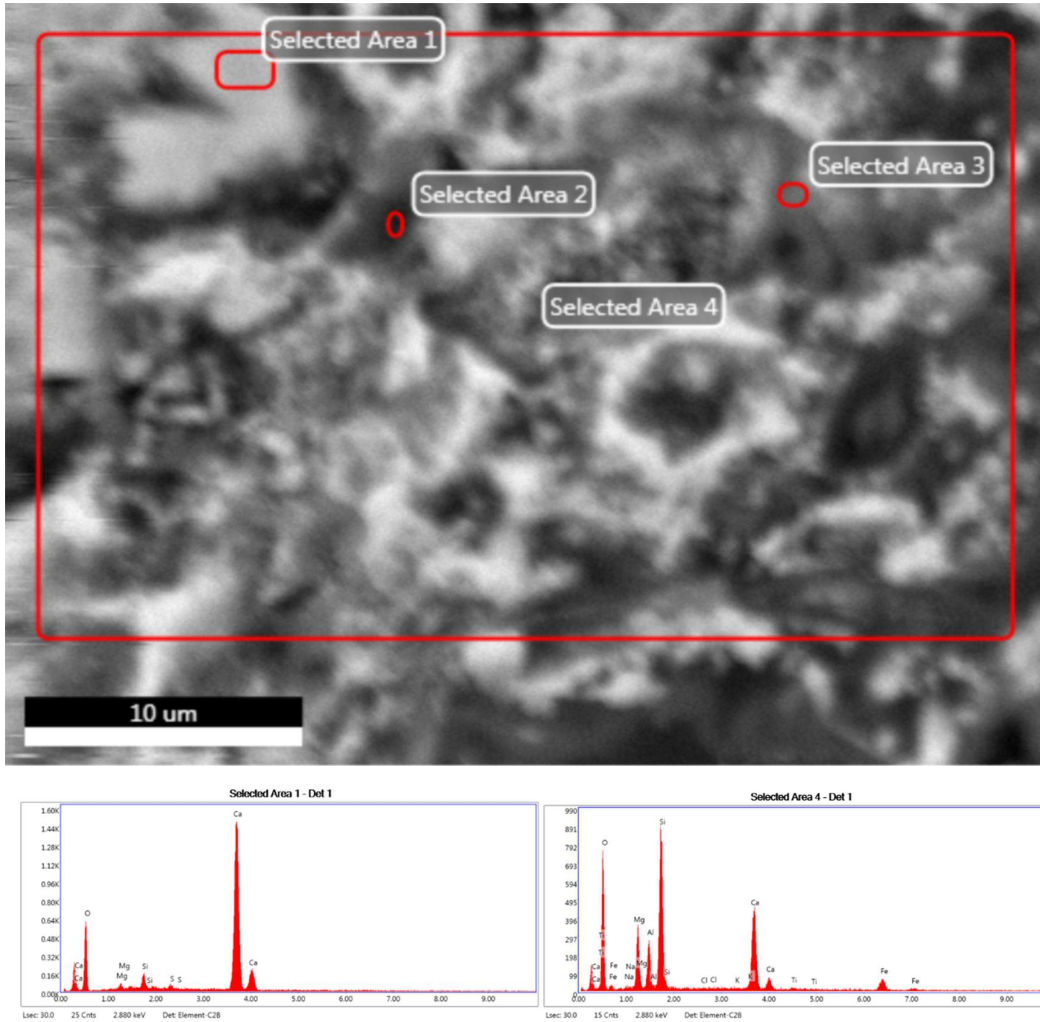


Figure 29: 5000x magnification of MG12 ceramic groundmass with infiltration of lime (area 1).

The ceramic aggregate is enriched in calcium throughout its micropores, shown in lighter tones (area 1). While the general chemistry of the probed area (area 4) shows Mg and Ca in almost equal proportions, it is evident that the calcium is present as a carbonate and not a hydrated phase like C-S-H. Darker tones within the secondary image signify the presence of M-S-H and other aluminum-rich phases. In zones where Ca is detected in high percentages, Si content is too low to suggest any C-S-H production.

4.4 Results of Binder Fractions

Three binder fractions (from MG01, MG05, and MG10) were prepared by wet gravimetric separation. Each sample was further processed for XRPD and SEM-EDS analysis. To improve chemical representation, each sample was analyzed in three distinct areas through EDS. The mean and standard deviation are used and interpreted as the best representation of the binder fraction (Table 8).

4.4.1 XRPD

The two groupings identified by optical microscopy carry into the mineralogical results of the binder fractions (Table 7).

Sample	Calcite	Vaterite	Monocarbonate	Quartz	Muscovite	Phyllosilicate Gels	Amorphous
MG01_B2	23.47	0.81	3.68	0.43	0.53	0.00	71.08
MG05_B2	22.55	1.87	2.44	0.34	0.46	0.00	72.34
MG10_B2	16.11	0.00	0.00	0.26	0.00	40.40	43.23

Table 7: XRPD results for the binder fractions. Binders from Group 1 present a higher calcite content, whereas the binder from Group 2 had very high percentage of phyllosilicate gels and a lower percentage of amorphous phase.

The monocarbonate in MG01_B2 and MG05_B2 alludes to the production of calcium aluminate hydrated phases (C-A-H) typical of pozzolanic reactions. The abundance of phyllosilicate gels from MG10_B2 likely stems from the magnesium content in the ceramic aggregate that could produce a paracrystalline magnesium silicate hydrate.

4.4.2 SEM-EDS

Binder fraction was extracted from samples MG01, MG05, and MG10 via wet gravimetric separation. These samples were chosen due to the high amorphous content calculated during XRPD analysis. Of them, MG01_B2 and MG05_B2 represent Group 1, identified microscopically by their volcanic breccia-rich makeup. MG10_B2 represents Group 2, the ceramic-rich mortars.

Mean								
Sample	Na ₂ O	MgO	Al ₂ O ₃	SiO ₂	P ₂ O ₅	K ₂ O	CaO	Fe ₂ O ₃
MG01_B2	4.24	4.69	11.82	46.61	3.53	0.88	25.80	2.42
MG05_B2	4.43	3.04	9.67	44.52	4.38	0.48	31.87	1.85
MG10_B2	2.76	16.49	8.55	50.09	2.32	0.52	18.03	1.25

Standard deviation								
Sample	Na ₂ O	MgO	Al ₂ O ₃	SiO ₂	P ₂ O ₅	K ₂ O	CaO	Fe ₂ O ₃
MG01_B2	0.43	0.31	0.38	0.30	0.15	0.06	1.06	0.17
MG05_B2	0.46	0.22	0.05	0.61	0.23	0.05	0.66	0.06
MG10_B2	0.04	0.42	0.07	0.19	0.18	0.07	0.33	0.22

Table 8: Standard deviation and mean of the calculated weight percentages of elements by sample from SEM-EDS.

The appearance of phosphate (P₂O₅) in the binder fractions is attributed to the anti-flocculant salt added during wet gravimetric separation and is not considered relevant to the study. Sodium is present both in the pozzolanic aggregates and in the anti-flocculant salt, so its relevancy is mixed. The MG01 binder fraction is low in magnesium with a disproportionate silica to calcium ratio. MG05 binder fraction presents a similar silica-rich matrix, unsurprising as they both derive from the *odeon* (Structure E). This suggests that part of the fine grained pozzolanic material remained unreacted, while the larger clasts initiated the crystallization of C-S-H and AFm phases. In the C-S-H, calcium and silicates are of equal proportion.

40% of the MG10_B2 binder fraction was comprised of phyllosilicate gels, likely identifiable as M-S-H, diverging from MG01_B2 and MG05_B2 which had no detected phyllosilicate gels. This is corroborated by the XRPD binder fraction results, where MG01_B2 and MG05_B2 have similar percentages of amorphous content (MG01: 71.1%, MG05: 72.3%) and calcite (MG01: 23.5%, Mg05: 22.5%), with small amounts of monocarbonate, vaterite, muscovite, and quartz.

MG01 Binder

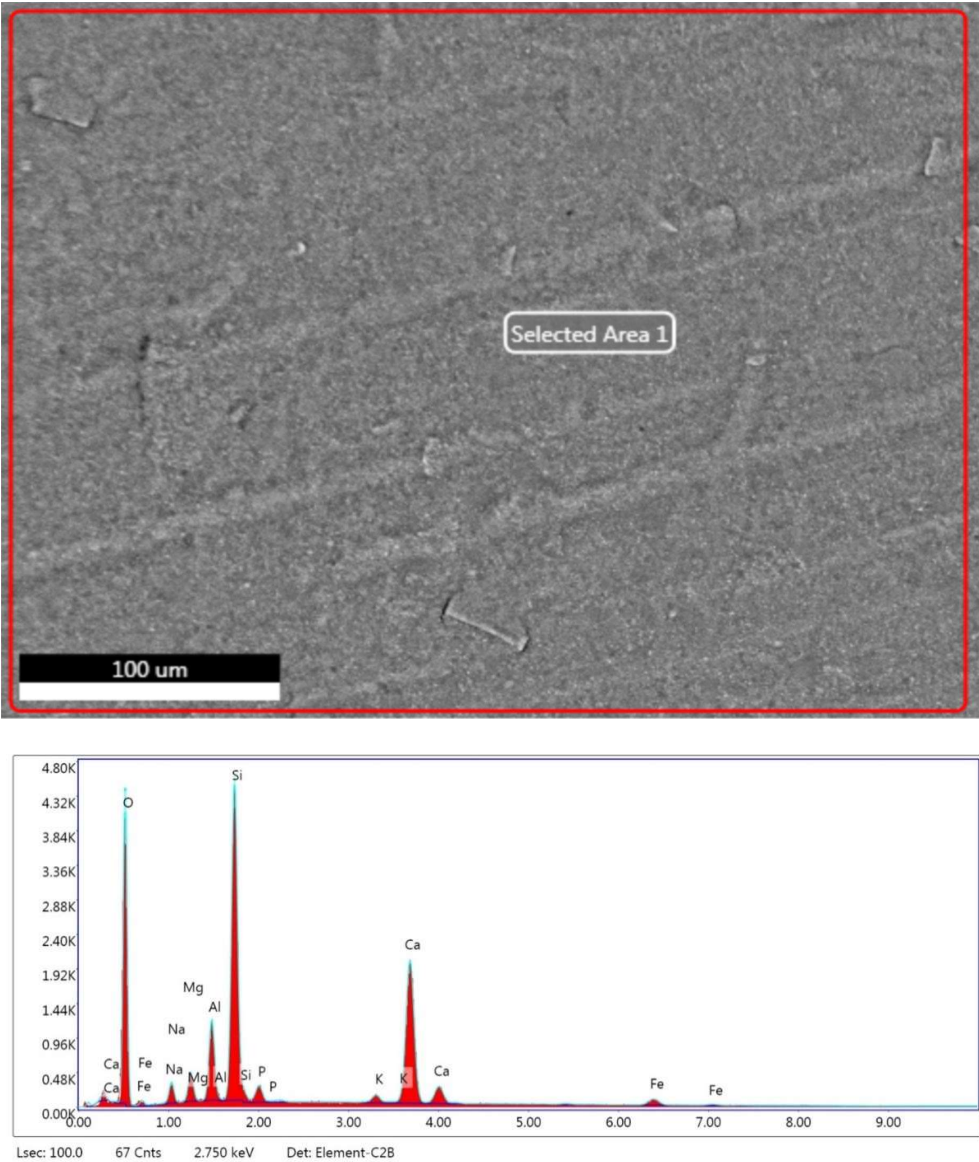


Figure 30: MG01 Binder Fraction at 500x magnification.

In MG01_B2, the high aluminum and silica content compared to calcium may stem from a C-A-H phase. The ratio of silica is in fact much more abundant than C-S-H ratio would require, suggesting a fine-grained pozzolanic ash exists in the binder fraction but remains unreacted. This powder could come directly from the volcanic breccia, which is quite friable.

MG05 Binder

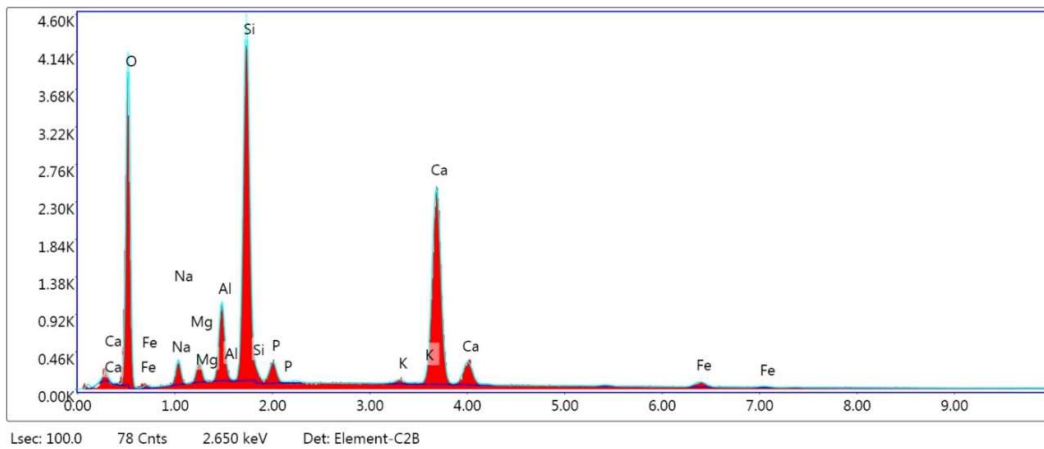
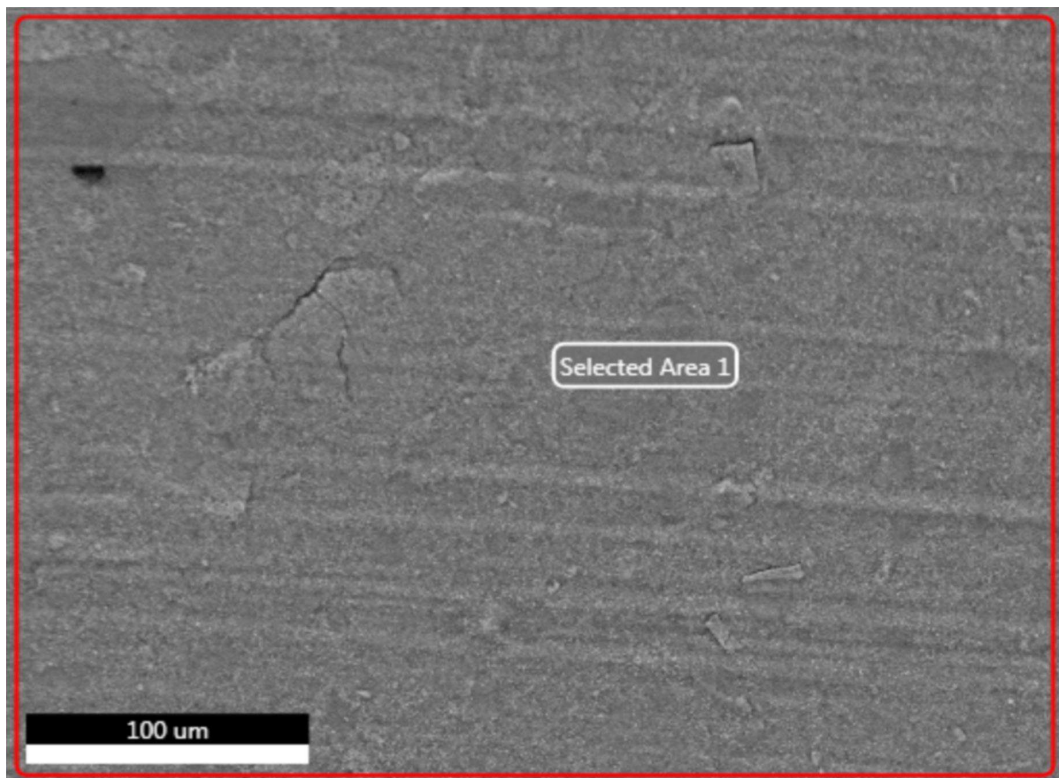


Figure 31: MG05 binder fraction at 500x magnification displays a strong peak of Si.

MG05_B2 is chemically alike and in the same elemental proportions as MG01_B2. Pozzolanic ash would certainly explain its relevant 72.34% amorphous content in XRPD. This would also account for the low quantity of iron detected, as both the breccias and the bulk mortar MG05 contained magnetite.

MG10 Binder

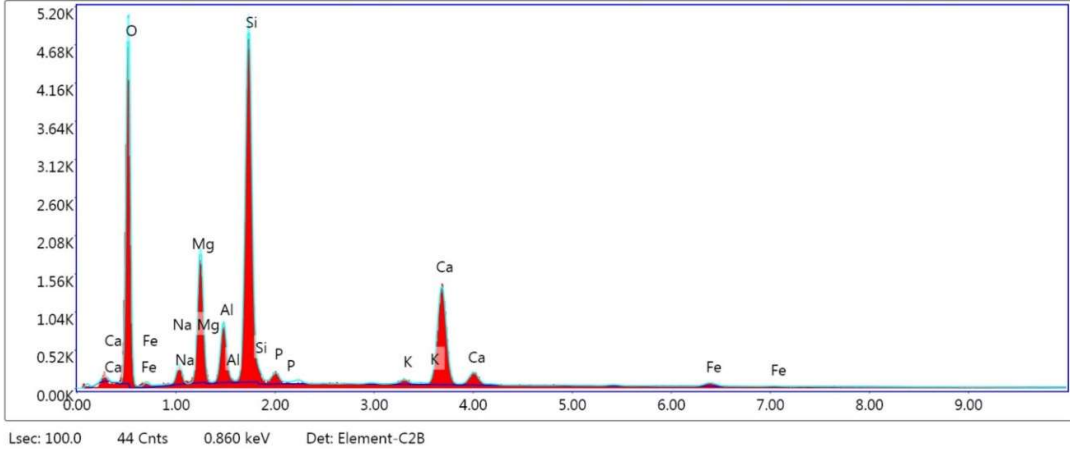
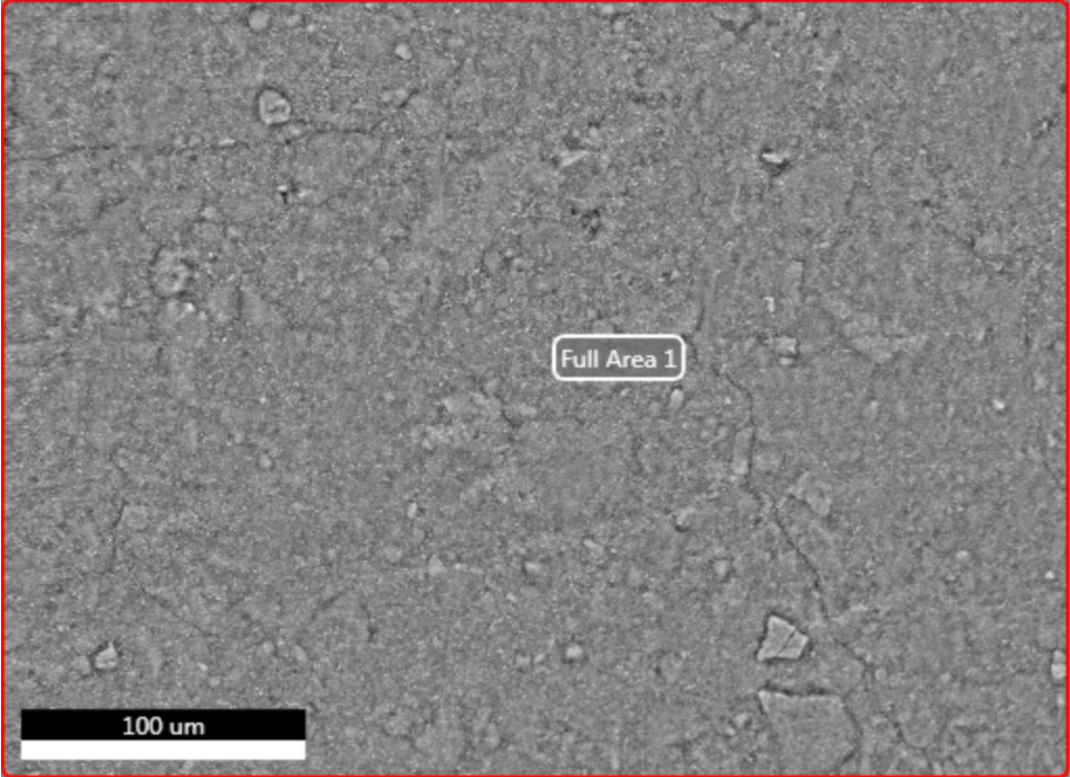


Figure 32: MG10 Binder fraction at 500x magnification. There is significantly more Mg in the system than in MG01 and MG05 binder fractions.

MG10_B2 has markedly lower calcite than its counterparts, and significantly higher magnesium content. It is evident that the ceramic-rich mortars have a completely different chemistry and reactive process than the breccia-rich mortars.

4.5 XRF

CLASTS	MG01_cl1	MG03_cl2	MG03_cl3	MG03_cl4	MG03_cl5	MG07_cl1	MG09_cl1	MG09_cl4
Na ₂ O	4.33	5.42	5.54	5.39	4.94	5.32	5.1	5.52
MgO	1.51	0.45	0.49	1.01	1.65	1.29	3.19	1.93
Al ₂ O ₃	16.6	16.61	16.65	16.58	18.12	17.76	18.21	18.07
SiO ₂	56.84	63.32	63.83	64.02	61.02	60.7	61.17	61.18
P ₂ O ₅	0.37	0.3	0.31	0.35	0.4	0.43	0.44	0.43
K ₂ O	2.66	4.43	4.71	4.45	3.21	3.48	3.34	3.79
CaO	13.22	5.69	4.6	2.47	5.26	6.19	4	3.67
TiO ₂	0.7	0.6	0.65	0.69	0.8	0.76	0.85	0.82
MnO	0.06	0.05	0.05	0.3	0.09	0.08	0.09	0.11
Fe ₂ O ₃	4.6	3.65	3.71	5.05	4.19	3.67	5.11	4.47
L.O.I.	12.99	4.41	3.64	2.98	8.08	7.48	8.37	6.39
PPM								
S	431	23	46	21	76	122	170	153
Sc	23	7	9	B.D.	10	11	7	6
V	65	11	10	21	30	26	32	29
Cr	B.D.	10	B.D.	B.D.	6	7	<6	B.D.
Co	B.D.	B.D.	B.D.	6	B.D.	B.D.	4	3
Ni	5	B.D.	B.D.	B.D.	B.D.	B.D.	3	B.D.
Cu	4	6	5	4	B.D.	B.D.	5	B.D.
Zn	100	145	120	123	127	108	249	131
Ga	11	15	16	15	19	19	20	15
Rb	58	124	129	123	90	77	70	86
Sr	852	556	481	421	795	764	872	807
Y	15	18	19	20	23	26	27	24
Zr	454	494	566	548	655	586	653	593
Nb	98	75	81	81	133	108	113	120
Ba	896	745	773	881	976	916	935	1056
La	72	59	65	65	104	100	86	99
Ce	145	109	119	135	198	191	170	192
Nd	50	38	48	48	57	59	51	50
Pb	11	13	9	16	9	8	11	14
Th	26	9	13	13	25	24	24	28
U	4	3	3	5	5	5	3	6

Table 9: XRF results in percentage (presented as oxides) and parts per million (PPM). B.D = below detection limit.

XRF was utilized for provenance determination by geochemical compositional comparison between selected volcanic aggregate samples and the geological reference database whose samples have a known origin. The geochemical fingerprints of the volcanic clasts mechanically removed from the mortars are reported on Table 9.

Scatterplots of the multivariate statistical processing for major and trace elements compare MG clasts with geological samples from the in-house geochemical database of Euganean Hill volcanic rocks. Among the breccia clasts selected from the mortars (MG01_c11, MG03_c15, MG07_c11, MG09_c11, MG09_c14) a high content of strontium ($\text{Sr} > 700$ ppm) was detected, a divergence from typical Euganean trachyte lavas whose Sr content is below 700 ppm (Brombin 2023). By using this element as a proxy, similar Sr trends were identified in the Villa Draghi breccia samples whose general chemistry appears to be more compatible with trachyandesite than true trachyte. Using bivariate scatterplots (Figure 33) of the concentration of Sr in comparison to other discriminant trace elements (Sr/Ba, Sr/Nb, Sr/Rd, Sr/Nd) previously adopted for geochemical provenance discrimination of Euganean volcanic rocks (Dilaria et al. 2024), many of the archeological samples fell within the intervals of the volcanic breccias of Villa Draghi. This peculiar abundance of trace strontium represents the site's unique geochemical fingerprint that is incompatible with other local Oligocene magmatic rocks (trachyte, latites and rhyolites), including other known breccias (both trachytic and rhyolitic) of the Euganean magmatic district.

Major elements also acted as discriminant proxies, as K_2O rates were extremely low in the breccia clasts, thus confirming the high concentration of plagioclases and low K-feldspar content first recognized under optical microscopy. By plotting K_2O concentration against SiO_2 , Al_2O_3 and Na_2O , one can observe the compatibility of Villa Draghi breccia samples and the clasts sampled from mortars (Figure 34). The remaining clasts (MG03_c2, MG03_c3, MG03_c4) can be firmly assigned as Euganean trachyte.

LDA processing provided the final proof of provenance for clasts MG01_c11, MG03_c15, MG07_c1, MG09_c11, MG09_c14. Based on a selection of discriminant major and trace elements (Na_2O , Al_2O_3 , SiO_2 , K_2O , TiO_2 , Sr, Zr, Nb, Ba), their origin is confirmed by an extremely high rate of correspondence ($> 95\%$) of the 1st probability to the Villa Draghi outcrop. The trachyte clasts (MG03_c2, MG03_c3, MG03_c4) had lower rates of correspondence, but probably derive from Monte Merlo and Monte Oliveto (Table 10).

Sample	Provenance	Probability (%)	Secondary Provenance	Secondary Probability (%)
MG01_clast1	Villa Draghi (Br)	100	M. Rosso	0
MG03_clast2	M. Merlo	73.04	M. Oliveto	26.94
MG03_clast3	M. Merlo	65.3	M. Oliveto	32.36
MG03_clast4	M. Oliveto	52.31	M. Lozzo	47.29
MG03_clast5	Villa Draghi (Br)	100	M. Trevisan	0
MG07_clast1	Villa Draghi (Br)	100	M. Merlo	0
MG09_clast4	Villa Draghi (Br)	99.68	M. Trevisan	0.32
MG09_clast1	Villa Draghi (Br)	100	M. Trevisan	0

Table 10: Discriminant analysis results of the aggregate clasts of Montegrotto Terme. Compared to geological samples of known provenance, the breccia clasts were identified as originating from the Villa Draghi quarry site.

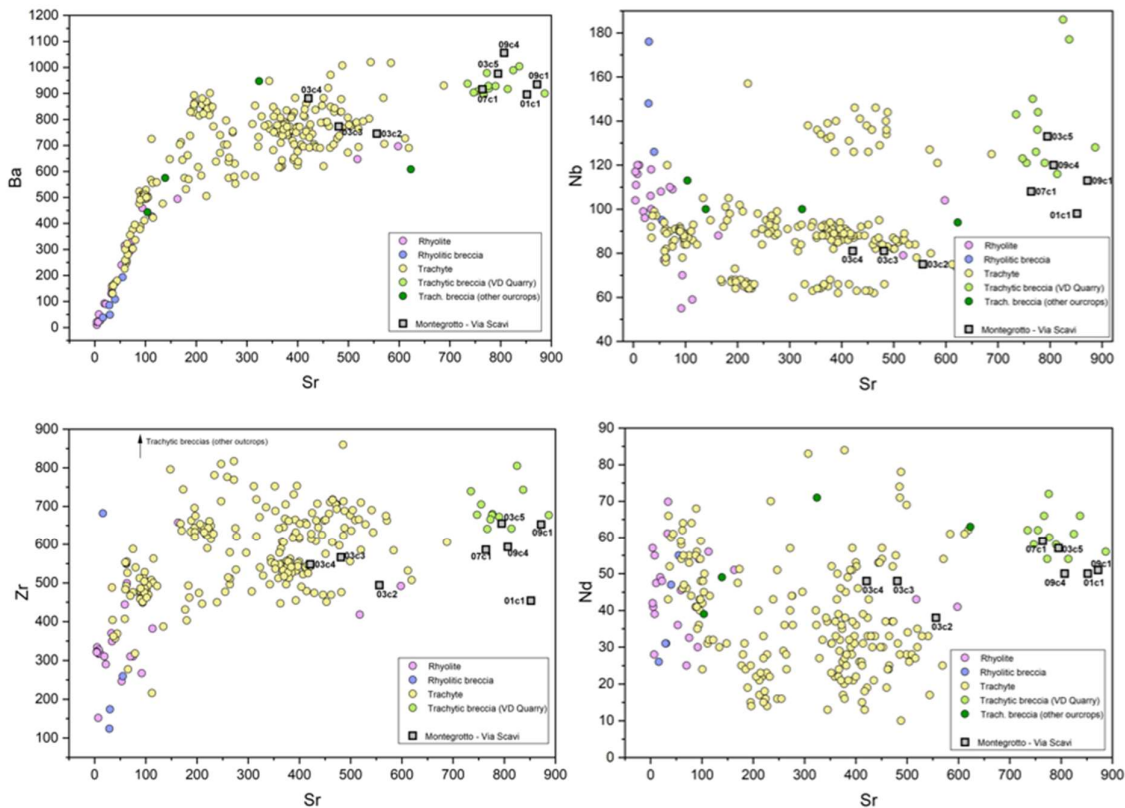


Figure 33: Multivariate scatterplots highlighting the relationships between trace elements Ba/Sr (top left), Nb/Sr (top right), Zr/Sr (bottom left), and Nd/Sr (bottom right). MG samples are represented as grey squares.

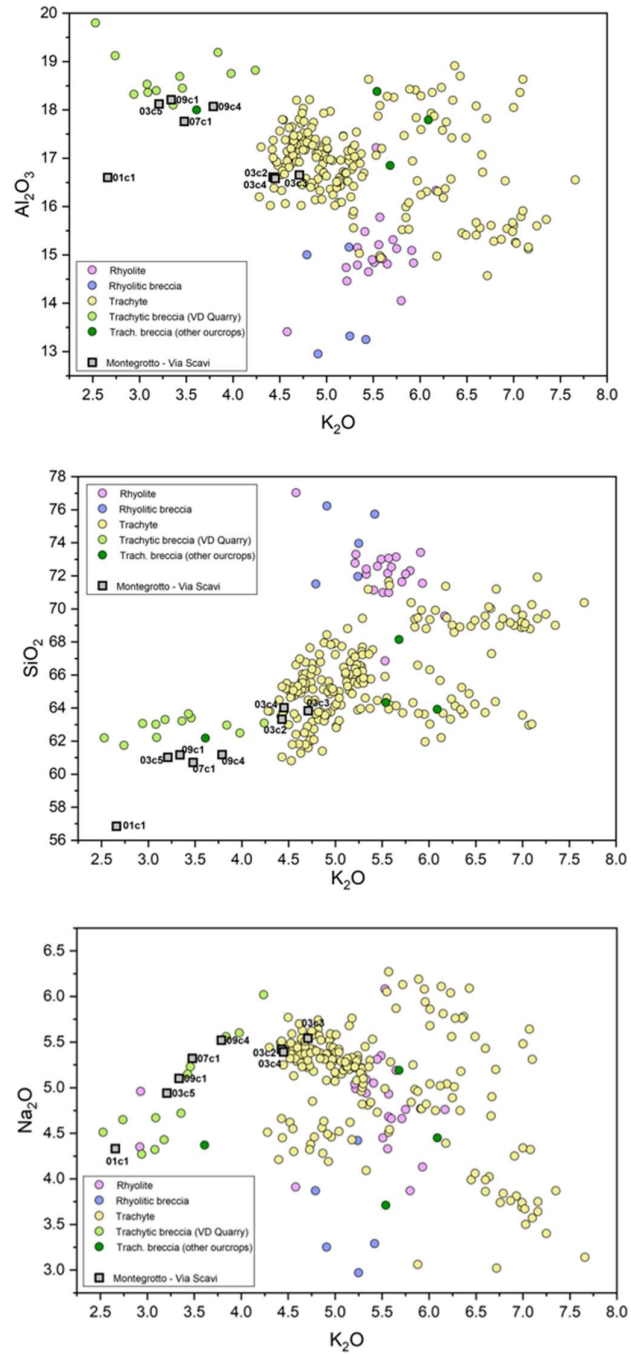


Figure 34: Scatterplots showing the abundance and relationship of Potassium compared to Sodium (Na), Silica (Si), and Aluminum (Al) expressed as oxides. Breccia samples from Villa Draghi are distinctively lower in potassium than their trachyte counterparts.

5. Discussion

The Via degli Scavi site is amongst many thermal complexes whose mortars have been studied in recent years. The thermal complex of Baia is close to the Mediterranean Sea and relies on ceramic fragments, pozzolana from the Phlegraean Fields of Campania, and trachytic pumice (Rispoli et al. 2019). Baia's local pozzolan happens to be the Vitruvian example, in part due to the importance of the region as a retreat for the elite of Rome, and due to its proximity to the fields where pozzolana was sourced. The Sarno baths of Pompeii also utilized pozzolans from the Phlegraean fields during the Imperial phases of construction, but earlier phases of the structure used foam lava (Secco et al. 2019). Modification of pozzolanic aggregate seems dependent on availability, and true Phlegraean pozzolana is not always deemed necessary.

The imperial age saw the import of Phlegraean pozzolan across the empire for large construction projects. It can be found in the structural mortars of the city of Nora in Sardinia (Dilaria et al. 2023) and is well documented in the mortars of Caesarea Maritima in Israel (Brandon et al. 2014).

The thermal retreat at Aquae Patavinae was probably not a candidate for Phlegraean pozzolan import for several reasons. Firstly, the local pozzolanic material was already known and exploited in construction projects, as it was available at the time of the thermal complex's construction. Secondly, while distance obviously did not inhibit the use of Phlegraean pozzolan, the imperial importance of the site is significantly lesser than the case studies presented previously. Members of the imperial family and the elite families of Rome used Baia as a resort town, and many similar thermal complexes dotted the landscape between Rome and its nearest neighboring cities. The Aquae Patavinae sites likely drew a more local crowd and perhaps never gained the attention of the heads of state beyond Tiberius' brief visit on campaign. Patavium was connected to the Adriatic Sea by a fluvial port, so transportation was certainly feasible. This leads to the conclusion that the pozzolana found in the Euganean Hills was of such a quality that no import was ever necessary.

The poor quality of MG08 and its divergence from the other samples leads to the conclusion that the structure was added at a much later stage of construction, with poorer materials. This lack of waterproofing binders may further indicate the structure's purpose; perhaps there was no concern of running water that would motivate a builder to use pozzolanic mortars.

A post-depositional challenge in interpreting the mineralogical properties and original composition of the mortars is caused by the leaching and potential re-precipitation of crystalline calcite. This prevalence of calcite-filled pores alludes to the humid environment of northern Italy and the pervasive thermal springs that exposed the soluble alkaline minerals to water for many centuries. The acclaimed “self-healing” properties of Roman concrete is a consequence of environmental conditions and mineralogical properties of the raw materials (Seymour et al. 2023). At present, there is no documentation that this characteristic was a known and intentional technological attribute of construction in antiquity; ironically, excess calcite or lime lumps were considered “poorly mixed” binders, as defined by Vitruvius (Vitr. 7.2.1).

The volcanic aggregates in breccia-rich mortars were provenanced by the statistical processing of XRF results. This technique was similarly used by Marra et al (2011) to determine the provenance of mortar elements, linking them to Monti Sabatini and the Alban Hills volcanic districts. The Alban hills have a higher potassium content than the Euganean ones, but the silicate is variable. This methodology shows the capability of XRF in relating archeological materials to their provenance and the categorization of geological resources by potential reactivity.

MG01, MG03, MG07, and MG09 all had at least one volcanic clast that matched the trachytic breccia sampled from Villa Draghi. Due to the physical limitation of the aggregate sizes and feasibility of extraction from bulk mortar, it was not possible to sample clasts from every breccia-rich mortar. Several clasts from MG03 matched with trachyte, proving that breccia was not exclusively used. It seems more probable that the trachyte was added as a repurposed industrial waste instead of an attempt to resource pozzolanic materials. The qualities of trachyte were known in the Roman world and the largescale use of Euganean trachyte likely created an abundance of quarry debris.

6. Conclusion

From petrographic and geochemical analysis, it is evident that the Romans utilized breccia from the Euganean Hills in the construction of the Via degli Scavi site. While the pools themselves use ceramics as a pozzolanic aggregate, the *odeon* (Structure E) and upper levels of pool structures (Structure C) rely on geological sources of pozzolan. Ultimately, this research reveals the predominant pozzolanic aggregates of the Via degli Scavi thermal complex originate from the Villa Draghi quarry site. Two pozzolanic sources were used, divided by function: volcanic breccia for structural purposes, and ceramics for waterproofing.

The limited representativeness of thin sections may require further extraction of archaeological mortar to ensure the total survey of the mortar types at Via degli Scavi. Comparison with the geological samples confirms the identity of diverse breccia and trachyte clasts. It is possible that further field surveys may uncover currently unknown ancient quarry sites within the Euganean Hills. In the future, one may be able to reconstruct the industrial pathways that built the ancient settlements surrounding the Euganean Hills, though it is likely most ancient quarries have been lost forever due to post-antiquity extraction industries. Further study may reveal connections between archaeological sites that can provide context of building phases throughout ancient *Patavium* and its periphery. This successful provenance has the potential to span across various archaeological contexts to create a chronology of pre-modern quarrying in the Euganean Hills.

Most clearly, this work shows the incredible knowledge of local natural resources in antiquity. The replication of this methodology to other sites in the region may one day reconstruct the overarching building trends of ancient *Patavium*.

7. References

- Addis, Anna, Michele Secco, Fabio Marzaioli, Gilberto Artioli, Alexandra Chavarría Arnau, Isabella Passariello, Filippo Terrasi, and Gian Pietro Brogiolo. “Selecting the Most Reliable 14C Dating Material Inside Mortars: The Origin of the Padua Cathedral.” *Radiocarbon* 61, no. 2 (April 2019): 375–93. <https://doi.org/10.1017/RDC.2018.147>.
- Barnes, P., and J. Bensted. *Structure and Performance of Cements, Second Edition*. CRC Press, 2002.
- Biblioteca Comunale Montegrotto Terme, Italia Soprintendenza archeologica per il Veneto, and Montegrotto Terme Assessorato alla cultura. *Delle antiche terme di Montegrotto: sintesi archeologica di un territorio*. Battaglia Terme: La galiverna, 1997.
- Bonetto, Jacopo, and Simone Dilaria. “Circolazione Di Maestranze e Saperi Costruttivi Nel Mediterraneo Antico. Il Caso Dei Rivestimenti in Malta Delle Cisterne Punico-Romane Di Nora, in ATTA, 31, Pp. 495-520.” *Atlante Tematico Di Topografia Antica*, January 1, 2021.
- Bonetto, Jacopo, Elena Pettenò, and Francesca Veronese. *Padova: la città di Tito Livio*. CLEUP, 2017.
- Brombin, Valentina. “Geochimica delle rocce magmatiche dei Colli Euganei (PD) e dei Monti Berici (VI),” April 27, 2023. <https://thesis.unipd.it/handle/20.500.12608/18208>.
- Capedri, Silvio, Riccardo Grandi, and Giampiero Venturelli. “Trachytes Used for Paving Roman Roads in the Po Plain: Characterization by Petrographic and Chemical Parameters and Provenance of Flagstones.” *Journal of Archaeological Science* 30, no. 4 (April 1, 2003): 491–509. <https://doi.org/10.1006/jasc.2002.0857>.
- Chiotis, Eustathios D., George Papadimitriou, S Tzoutzopoulos, and E Dimou. “A Study of Some Ancient and Prehistoric Plasters and Watertight Coatings from Greece.” *Archaeometry Issues in Greek Prehistory and Antiquity*, 2001.
- Columbu, Stefano, Anna Maria Garau, and Carlo Lugliè. “Geochemical Characterisation of Pozzolanic Obsidian Glasses Used in the Ancient Mortars of Nora Roman Theatre (Sardinia, Italy): Provenance of Raw Materials and Historical–Archaeological Implications.” *Archaeological and Anthropological Sciences* 11, no. 5 (May 1, 2019): 2121–50. <https://doi.org/10.1007/s12520-018-0658-y>.
- Cucato, M. “Carta Geologica D’Italia—Padova Sud—Foglio, 147, 1:50000.” 1:50000. Florence, Italy: Servizio geologico d’Italia, 2011. https://www.isprambiente.gov.it/Media/carg/147_PADOVA_SUD/Foglio.html.

- Deiana, Rita, and Caterina Previato. “Geophysical Surveys for Archaeological Research in Urban Areas: The Case of the Roman Theatre in Padua.” *Heritage* 6, no. 2 (February 2023): 946–56. <https://doi.org/10.3390/heritage6020052>.
- Dilaria, Simone, Jacopo Bonetto, Luigi Germinario, Caterina Previato, Chiara Girotto, and Claudio Mazzoli. “The Stone Artifacts of the National Archaeological Museum of Adria (Rovigo, Italy): A Noteworthy Example of Heterogeneity.” *Archaeological and Anthropological Sciences* 16, no. 1 (January 2024): 14.
- Dilaria, Simone, Michele Secco, Andrea R. Ghiotto, Guido Furlan, Tommaso Giovanardi, Federico Zorzi, and Jacopo Bonetto. “Early Exploitation of Neapolitan Pozzolan (Pulvis Puteolana) in the Roman Theatre of Aquileia, Northern Italy.” *Scientific Reports* 13, no. 1 (March 13, 2023): 4110.
- Dilaria, Simone, Caterina Previato, Jacopo Bonetto, Michele Secco, Arturo Zara, Raffaella Luca, and Domenico Miriello. “Volcanic Pozzolan from the Phlegraean Fields in the Structural Mortars of the Roman Temple of Nora (Sardinia).” *Heritage* 6 (January 10, 2023): 567–86. <https://doi.org/10.3390/heritage6010030>.
- Dilaria, Simone, and Michele Secco. “Mortar Recipes Through the Ages. A Brief Review of Data from Prehistory to Late Antiquity.” *Arheologija i Prirodne Nauke* 18 (December 15, 2022). https://doi.org/10.18485/arhe_apn.2022.18.9.
- Gasparotto, Cesira. *Patavium municipio romano / C. Gasparotto*. Venezia: a spese della R. Deputazione, 1928.
- Germinario, Luigi, Siegfried Siegesmund, Lara Maritan, and Claudio Mazzoli. “Petrophysical and Mechanical Properties of Euganean Trachyte and Implications for Dimension Stone Decay and Durability Performance.” *Environmental Earth Sciences* 76, no. 21 (October 29, 2017): 739. <https://doi.org/10.1007/s12665-017-7034-6>.
- Katayama, Tetsuya. “The So-Called Alkali-Carbonate Reaction (ACR) — Its Mineralogical and Geochemical Details, with Special Reference to ASR.” *Cement and Concrete Research*, January 1, 2010.
- Kim, Gyeongryul, Sumin Im, Hyeonseok Jee, Heongwon Suh, Seongmin Cho, Manabu Kanematsu, Satoshi Morooka, et al. “Effect of Magnesium Silicate Hydrate (M-S-H) Formation on the Local Atomic Arrangements and Mechanical Properties of Calcium Silicate Hydrate (C-S-H): In Situ X-Ray Scattering Study.” *Cement and Concrete Research* 159 (September 1, 2022): 106869.

- Le Bas, M. J., and A. L. Streckeisen. “The IUGS Systematics of Igneous Rocks.” *Journal of the Geological Society* 148, no. 5 (September 1991): 825–33. <https://doi.org/10.1144/gsjgs.148.5.0825>.
- Leone, Gemma, Alessandra De Vita, Marco Consumi, Gabriella Tamasi, Claudia Bonechi, Alessandro Donati, Claudio Rossi, and Agnese Magnani. “Comparison of Original and Modern Mortars at the Herculaneum Archaeological Site.” *Conservation and Management of Archaeological Sites* 21, no. 2 (March 4, 2019): 92–112. <https://doi.org/10.1080/13505033.2019.1638139>.
- Maravelaki-Kalaitzaki, Pagona, Asterios Bakolas, and A. Moropoulou. “Physico-Chemical Study of Cretan Ancient Mortars.” *Cement and Concrete Research* 33 (May 1, 2003): 651–61. [https://doi.org/10.1016/S0008-8846\(02\)01030-X](https://doi.org/10.1016/S0008-8846(02)01030-X).
- Maritan, Lara, Giovanna Ganzarolli, Fabrizio Antonelli, Manuel Rigo, Angeliki Kapatza, Katalin Bajnok, Chiara Coletti, et al. “What Kind of Calcite? Disclosing the Origin of Sparry Calcite Temper in Ancient Ceramics.” *Journal of Archaeological Science* 129 (May 1, 2021): 105358. <https://doi.org/10.1016/j.jas.2021.105358>.
- Maritan, Lara, Claudio Mazzoli, Raffaele Sassi, Fabio Speranza, Angela Zanco, and Paola Zanovello. “Trachyte from the Roman Aqueducts of Padua and Este (North-East Italy): A Provenance Study Based on Petrography, Chemistry and Magnetic Susceptibility.” *European Journal of Mineralogy*, September 13, 2013, 415–27. <https://doi.org/10.1127/0935-1221/2013/0025-2282>.
- Moropoulou, A., A. Bakolas, and K. Bisbikou. “Characterization of Ancient, Byzantine and Later Historic Mortars by Thermal and X-Ray Diffraction Techniques.” *Thermochimica Acta*, Recent Advances in Thermal Analysis and Calorimetry, 269–270 (December 20, 1995): 779–95. [https://doi.org/10.1016/0040-6031\(95\)02571-5](https://doi.org/10.1016/0040-6031(95)02571-5).
- Pecchioni, Elena, F. Fratini, and E. Cantisani. *Atlante delle malte antiche in sezione sottile al microscopio ottico- Atlas of the ancient mortars in thin section under optical microscope*. ITA, 2014. <https://flore.unifi.it/handle/2158/937731>.
- Rispoli, Concetta, Alberto De Bonis, Vincenza Guarino, Sossio Fabio Graziano, Claudia Di Benedetto, Renata Esposito, Vincenzo Morra, and Piergiulio Cappelletti. “The Ancient Pozzolan Mortars of the Thermal Complex of Baia (*Campi Flegrei*, Italy).” *Journal of Cultural Heritage*, Multidisciplinary study of the Sarno Baths in Pompeii, 40 (November 1, 2019): 143–54. <https://doi.org/10.1016/j.culher.2019.05.010>.
- Secco, Michele, Simone Dilaria, Jacopo Bonetto, Anna Addis, Sergio Tamburini, Nereo Preto, Giulia Ricci, and Gilberto Artioli. “Technological Transfers in the Mediterranean

- on the Verge of Romanization: Insights from the Waterproofing Renders of Nora (Sardinia, Italy).” *Journal of Cultural Heritage* 44 (July 1, 2020): 63–82. <https://doi.org/10.1016/j.culher.2020.01.010>.
- Secco, Michele, Luca Valentini, and Anna Addis. “Ancient and Modern Binders: Naturally Nanostructured Materials,” 205–37, 2018. <https://doi.org/10.1016/B978-0-12-813910-3.00010-0>.
- Seymour, Linda, Janille Maragh, Paolo Sabatini, Michel Tommaso, James Weaver, and Admir Masic. “Hot Mixing: Mechanistic Insights into the Durability of Ancient Roman Concrete.” *Science Advances* 9 (January 6, 2023): eadd1602. <https://doi.org/10.1126/sciadv.add1602>.
- Sinopoli, Anna, and Danila Aita. “The Dome of the Temple of Diana in Baiae: Opus Caementicium, Geometry and Mechanics.” *International Journal of Architectural Heritage* 16, no. 8 (August 3, 2022): 1152–83. <https://doi.org/10.1080/15583058.2020.1870777>.
- Štukovnik, P., V. Bokan Bosiljkov, and M. Marinšek. “Detailed Investigation of ACR in Concrete with Silica-Free Dolomite Aggregate.” *Construction and Building Materials* 216 (August 20, 2019): 325–36. <https://doi.org/10.1016/j.conbuildmat.2019.04.260>.
- Turchetto, Jacopo. “The Roman Centuriations of Patavium and Altinum A Water Management System in the Central Venetian Plain.” Engramma, August 2023. https://www.engramma.it/eOS/index.php?id_articolo=5223.
- Tykot, Robert H. “Obsidian Studies in the Prehistoric Central Mediterranean: After 50 Years, What Have We Learned and What Still Needs to Be Done?” *Open Archaeology* 3, no. 1 (October 26, 2017): 264–78. <https://doi.org/10.1515/opar-2017-0018>.
- Yegül, Fikret K. “The Thermo-Mineral Complex at Baiae and De Balneis Puteolanis.” *The Art Bulletin* 78, no. 1 (March 1, 1996): 137–61. <https://doi.org/10.1080/00043079.1996.10786675>.
- Zampieri, Girolamo. *Il Museo Archeologico Di Padova*. Electa, 1994. <https://www.lafeltrinelli.it/museo-archeologico-di-padova-girolamo-libri-vintage-girolamo-zampieri/e/2566891880414>.
- Zara, Arturo. *La trachite euganea: archeologia e storia di una risorsa lapidea del Veneto antico* / Arturo Zara. Roma: Quasar, 2018.

7.1 Ancient Sources:

- Henderson, Jeffrey. "Pliny Natural History: Book XXXI: Chapter XXXIII." Loeb Classical Library. Accessed October 21, 2023. https://www.loebclassics.com/view/pliny_elder-natural_history/1938/pb_LCL418.417.xml?readMode=reader.
- "LacusCurtius: Pliny the Elder's Natural History." n.d. Accessed March 26, 2023. https://penelope.uchicago.edu/Thayer/L/Roman/Texts/Pliny_the_Elder/31*.html.
- "LacusCurtius: Strabo's Geography — Book V Chapter 1." n.d. Accessed March 26, 2023. https://penelope.uchicago.edu/Thayer/E/Roman/Texts/Strabo/5A*.html.
- "C. Suetonius Tranquillus, Tiberius, Chapter 14." Accessed March 26, 2023. <https://www.perseus.tufts.edu/hopper/text?doc=Suet.+tib.+14&fromdoc=Perseus%3Atext%3A1999.02.0132>.
- "P. Vergilius Maro, Aeneid, Book 1, Line 223." Accessed May 13, 2024. <https://www.perseus.tufts.edu/hopper/text?doc=Perseus%3Atext%3A1999.02.0054%3Abook%3D1%3Acard%3D223>.
- Pollio, Vitruvius. 2016. *Vitruvii De architectura libri decem*. Edited by Valentin Rose. <https://www.gutenberg.org/ebooks/51812>.

8. List of Figures

Figure 1: Topographic map of Italy with the Veneto shaded in pink and the Euganean Hills marked in white.....	7
Figure 2: Morphological map of the Euganean Hills with the known Roman archeological sites of Patavium and Aquae Patavinae marked in blue. Two potential ancient quarry sites, Villa Draghi and Catajo, are marked by red diamonds. The Euganean hills are to the southwest of modern Padova and west of the Venetian Lagoon.	8
Figure 3: Satellite imagery of northern Italy with Roman city names highlighted.	9
Figure 4: Map of the Villa Draghi quarry (red) in relation to archaeological sites of Montegrotto Terme (blue).....	14
Figure 5: Photos of the newly discovered Villa Draghi quarry site by author	15
Figure 6: hypothetical reconstruction of the Via degli Scavi archeological site	19
Figure 7: The Site of Via degli Scavi, the ancient Fons Aponi	20
Figure 8: Hypothetical reconstruction of Via degli Scavi site, bottom with sampling points superimposed.....	20
Figure 10: Sampling of Villa Draghi Quarry, photos by S. Dilaria 2023	24
Figure 11: volcanic breccia-rich mortars (left to right: MG01, MG02, and MG04) in polarized light (PL) (top) and cross-polarized light (XPL) (bottom). These samples represent structure E. The base of each image is 3.6 cm.	32
Figure 12: MG02 (left) and MG04 (right) under PL (top) and XPL (bottom). In XPL, the distinction between trachyte and trachytic breccia is clear. The trachyte groundmass has a high degree of crystallinity and a lesser amorphous component, limiting its potential reactivity with the lime binder. In contrast, breccias present a crypto-crystalline, amorphous groundmass that greatly influences its potential reaction with lime binder. Phenocrysts are primarily constituted by plagioclases (sometimes agglomerated in glomerophyrs).	34
Figure 13: breccia clast from MG09 in XPL (left) and PL (right).....	34
Figure 14: MG04. Left: Volcanic aggregate under XPL. The aggregate shows thin phenocrysts of alkali feldspars (white, brown) and a large opaque mineral with high metallic content (black). A visible discoloration of the surrounding binder matrix represents the reaction rim of C-S-H production. Circular voids in the matrix are lined with crystalline calcite. Right: Volcanic aggregate in PL. The angularity of the top right	

aggregate may hint to intentional crushing of trachyte, to be confirmed in later geochemical analysis of aggregate clasts.....35

Figure 15: MG02 under XPL, depicting breccia and ceramic aggregate within a fat micritic binder.35

Figure 16: Sample MG10 (left) and MG12 (right) under PL (top) and XPL (bottom). The base of each figure measures 3.6 cm.36

Figure 17: MG10 under XPL. Left: the thick reaction rim (light brown) surrounding the ceramic fragment suggests a high concentration of a hydrated silicate phase. Right: the central, darker matrix with higher fine aggregate is a clast of mortar that has been reused as an aggregate.37

Figure 18: Sample MG12 under XPL. The capillary pores are filled with crystalline calcite. Abundant fine sands of quartzite and chert contrast the coarser ceramic fragments.....37

Figure 19, above: MG08 thin section in PL and XPL. The base of each figure measures 3.6 cm.....38

Figure 20, left: Sample MG08 under XPL. Three terracotta fragments are visible (upper and center right), alongside plentiful quartzite sands and a very large lime lump (top left).....38

Figure 21: SEM of MG02 at 500x magnification. Areas of high pozzolanic reactivity appear within the binder matrix.43

Figure 22: MG02 at 500x magnification. Areas 1 and 2 represent a breccia clast, and areas 3 and 4 are part of the reaction rim.....44

Figure 23: MG11 aggregates of siliceous and dolomitic sands as well as volcanic breccia at 100x magnification. The phenocrysts and holocrystalline matrix of the breccia aggregate are visible (area 7).....45

Figure 24: EDS results from area surveys of MG11 aggregates. Areas 2 and 5 appear to be dolomitic sands while areas 7 and 8 are volcanic breccia.46

Figure 25: MG11 breccia clast at 100x magnification. Phenocrysts and pores are distinguishable due to their varying atomic weights, lighter crystals equate to heavier minerals. This breccia is dominated by aluminum-rich silicates.....47

Figure 26: MG10 ceramic fragment matrix at 100x magnification and corresponding EDS chart.48

Figure 27: MG10, area with ceramic fragment and reaction rim at 100x magnification.49

Figure 28: MG12 at 1000x magnification, focused on the binder matrix. The ratio of Mg and Ca in the system allude to both M-S-H and C-S-H formation.50

Figure 29: 5000x magnification of MG12 ceramic groundmass with infiltration of lime (area 1).51

Figure 30: MG01 Binder Fraction at 500x magnification.54

Figure 31: MG05 binder fraction at 500x magnification displays a strong peak of Si.55

Figure 32: MG10 Binder fraction at 500x magnification. There is significantly more Mg in the system than in MG01 and MG05 binder fractions.56

Figure 33: Multivariate scatterplots highlighting the relationships between trace elements Ba/Sr (top left), Nb/Sr (top right), Zr/Sr (bottom left), and Nd/Sr (bottom right). MG samples are represented as grey squares.....59

Figure 34: Scatterplots showing the abundance and relationship of Potassium compared to Sodium (Na), Silica (Si), and Aluminum (Al) expressed as oxides. Breccia samples from Villa Draghi are distinctively lower in potassium than their trachyte counterparts.60

9. List of Tables

Table 1: Chart of sampling context.....	23
Table 2: samples within the UNIPD proprietary database of the Euganean Hills.....	30
Table 3: Thin sections reviewed under optical microscopy and categorized by coarse aggregate.....	31
Table 4: Mineralogical composition of bulk mortar samples from XRPD analysis. Amorph=amorphous, CAL=calcite, ARG=aragonite, VT=vaterite, MC=monocarbonate, DL=dolomite, QTZ=quartz, AND=andesine, OLG=Oligoclase, ANR=anorthoclase, SN=sanidine, MSC=muscovite, BIO=biotite CLNO=clinochlore, DIO=diopside, HNB=hornblende, HMT=hematite, MGT=magnetite, ANC=analcime ILM=ilmenite, PS Gels=phyllosilicate gels.....	39
Table 5: XRPD results for archaeological clasts and geological samples. CAL=calcite, VT=vaterite, MC=monocarbonate, DL=dolomite, QTZ=quartz, CRY=cristobalite, AND=andesine, ANR=anorthoclase, SN=sanidine, MSC=muscovite, BIO=biotite, CLNO=clinochlore, HNB=hornblende, MGT=magnetite, TRD= tridymite, GPS=gypsum, PS Gels=phyllosilicate gels, Amorph=amorphous.....	41
Table 6: Thin Sections chosen for SEM, with indicated the weight percentages of calcite and amorphous phase calculated through Rietveld refinement from XRPD.....	42
Table 7: XRPD results for the binder fractions. Binders from Group 1 present a higher calcite content, whereas the binder from Group 2 had very high percentage of phyllosilicate gels and a lower percentage of amorphous phase.	52
Table 8: Standard deviation and mean of the calculated weight percentages of elements by sample from SEM-EDS.	53
Table 9: XRF results in percentage (presented as oxides) and parts per million (PPM). B.D = below detection limit.....	57
Table 10: Discriminant analysis results of the aggregate clasts of Montegrotto Terme. Compared to geological samples of known provenance, the breccia clasts were identified as originating from the Villa Draghi quarry site.....	59